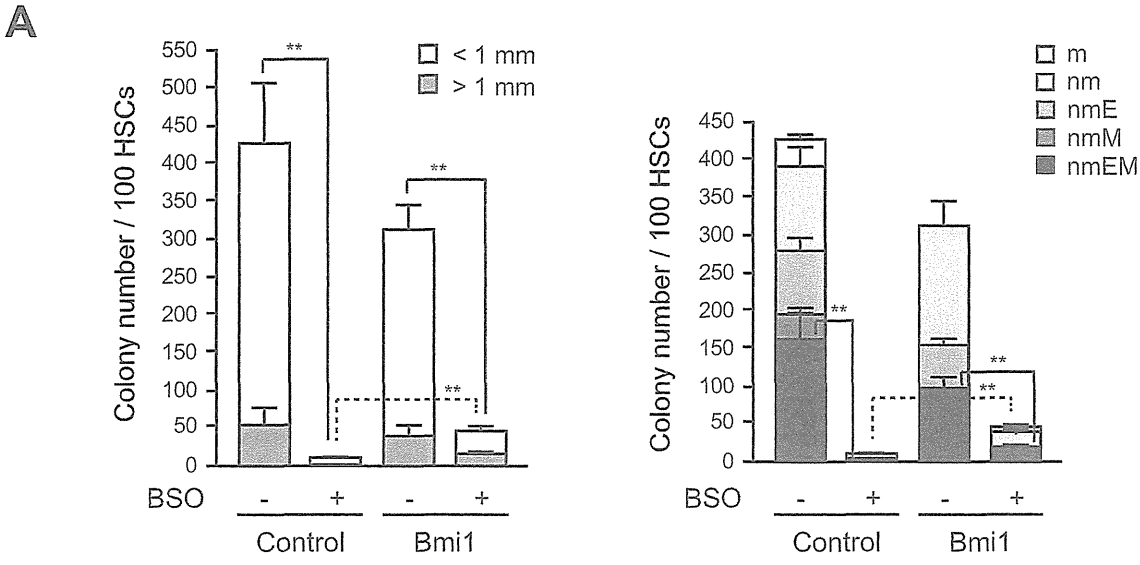
A
Colony number / 100 HSCs
< 1 mm
> 1 mm
m
nm
nmE
nmM
nmEM
BSO
Control
Bmi1

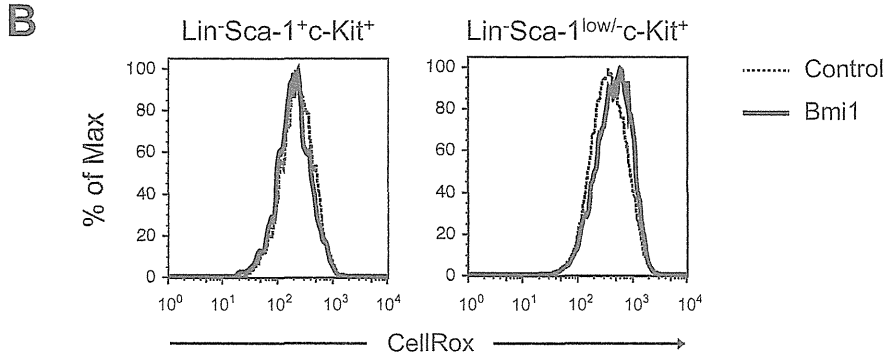
B
Lin-Sca-1+c-Kit+
Lin-Sca-1low/-c-Kit+
% of Max
Control
Bmi1
CellRox

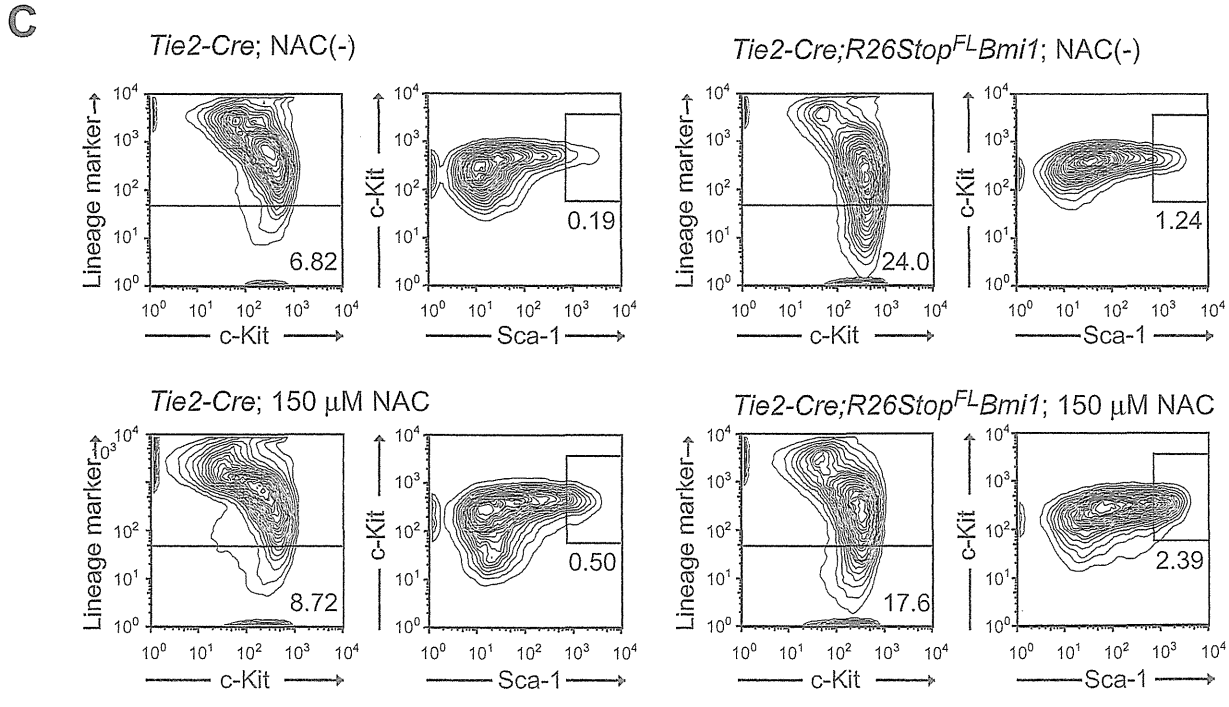
C
Tie2-Cre; NAC(-)
Tie2-Cre;R26StopFLBmi1; NAC(-)
Tie2-Cre; 150 μM NAC
Tie2-Cre;R26StopFLBmi1; 150 μM NAC
Lineage marker
c-Kit
Sca-1
6.82
0.19
24.0
1.24
8.72
0.50
17.6
2.39

Figure 6. Overexpression of Bmi1 confers oxidative stress on HSCs. (A) Colony formation by HSCs cultured for 3 days. $CD34^-LSK$ cells from *Tie2-Cre* (Control) and *Tie2-Cre;R26Stop^{FL}Bmi1* (Bmi1) mice were cultured in the SF-O3 serum-free medium supplemented with 50 ng/ml SCF, TPO and 0.05 mM of BSO. At day 3 of culture, the cells were plated in methylcellulose medium to allow formation of colonies in the presence of 20 ng/ml SCF, 20 ng/ml TPO, 20 ng/ml IL-3, and 3 u/ml EPO. Absolute numbers of LPP and HPP-CFCs (left panel) are shown as the mean ± S.D. for triplicate cultures. Absolute numbers of each colony types are shown in the right panel. Data are shown as the mean ± S.D. for triplicate analyses. Statistical analyses were performed on the total colony numbers (left panel) and nmEM colony numbers (right panel), respectively. $^{**}p<0.01$. (B) Levels of ROS in cells overexpressing *Bmi1*. $CD34^-LSK$ cells from *Tie2-Cre* (Control) and *Tie2-Cre;R26Stop^{FL}Bmi1* (Bmi1) mice were cultured in the SF-O3 serum-free medium supplemented with 50 ng/ml SCF and TPO. Representative flow cytometric profiles of LSK and Lineage marker$^-$Sca-1$^{low/-}$c-Kit$^+$ cells in cultures at day 14 are depicted. (C) Effects of NAC on *Bmi1* culture. $CD34^-LSK$ cells from *Tie2-Cre* and *Tie2-Cre;R26Stop^{FL}Bmi1* mice were cultured in the SF-O3 serum-free medium supplemented with 50 ng/ml SCF and TPO in the presence and absence of 150 μM NAC. Representative flow cytometric profiles of LSK cells in cultures at day 14 are depicted. The proportion of Lin^- and LSK cells in total cells are indicated.
doi:10.1371/journal.pone.0036209.g006

[27,28]. Together, this accumulating evidence suggests that Bmi1 is dynamically regulated in response to oxidative stress, probably downstream of p38. Our preliminary data demonstrated that activated p38 directly phosphorylates Bmi1 *in vitro* (Oshima and Iwama., unpublished data). Thus, it is possible that p38, which is activated by oxidative stress, attenuates Bmi1 function via direct phosphorylation of Bmi1. How oxidative stress restricts the expression and function of Bmi1 is an important issue to be addressed.

Of note, the effect of Bmi1 overexpression in serial transplantation resembles that of overexpression of *Ezh2*, a gene encoding a core component of PRC2 [29]. Overexpression of PcG genes, *Bmi1* and *Scmh1*, also induces tolerance of cortical neurons to ischemia [30]. Thus, various cellular stresses may target PcG complexes to release transcriptional repression of PcG-regulated genes, such as tumor suppressor and developmental regulator genes, thereby affecting stemness. All these findings support the notion that enforcement of PcG function is a key for successful regenerative therapies.

Meanwhile, the role of PcG proteins in resistance to oxidative stress is also implicated in cancer. Expression of PcG proteins including *BMI1* and *EZH2* are often up-regulated in various cancers, particularly in their cancer stem cell fractions [31]. Interestingly, cancer stem cells in some tumors appear to be susceptible to ROS, similar to normal stem cells, and thus develop mechanisms to keep the levels of ROS low [32]. Interference of EZH2 function by the small-molecule histone methyltransferases inhibitor, DZNep, is reported to increase ROS levels in acute myeloid leukemia cells like in *Bmi1*-deficient mice [33]. Conversely, our findings in this study suggest that an excess of PcG proteins often observed in aggressive cancer could help cancer stem cells tolerate oxidative stress. In this regard, overexpression of PcG proteins could also be therapeutic targets in cancers including leukemia. Finally, no *Tie2-Cre;R26Stop^{FL}Bmi1* mice developed hematological malignancies during the observation period, up to 18 months after birth. Only one recipient mice with *Tie2-Cre;R26Stop^{FL}Bmi1* BM cells developed acute lymphocytic leukemia in the tertiary transplantation. These findings suggest that Bmi1 by itself is not sufficient to induce hematological malignancies.

Methods

Ethics Statement

All experiments using the mice were performed in accordance with our institutional guidelines for the use of laboratory animals and approved by the review board for animal experiments of Chiba University (approval ID: 21–150).

Generation of Mice

To generate tissue-specific *Bmi1*-transgenic mice, we used the plasmid *R26Stop^{FL}*, a modified version of pROSA26-1 with a *loxP*-flanked *neo^r*-stop cassette, an *frt*-flanked *IRES-eGFP* cassette, and a bovine polyadenylation sequence [34]. We cloned a cDNA encoding a flag-tagged *Bmi1* upstream of the *IRES* sequence (*R26Stop^{FL}Bmi1*). R1 ES cells were transfected, cultured, and selected as previously described [35]. For conditional expression of *Bmi1*, the *RosaStop^{FL}Bmi1* mice were crossed with *Tie2-Cre* mice. C57BL/6 (CD45.2) mice were purchased from Japan SLC (Shizuoka, Japan). C57BL/6 mice congenic for the Ly5 locus (CD45.1) were purchased from Sankyo-Lab Service (Tsukuba, Japan). Mice were bred and maintained in the Animal Research Facility of the Graduate School of Medicine, Chiba University in accordance with institutional guidelines. This study was approved by the institutional review committees of Chiba University (approval numbers 21–65 and 21–150).

Flow Cytometric Analysis and Cell Sorting

Mouse $CD34^-LSK$ HSCs were purified from BM of 8–12-week-old mice. Mononuclear cells were isolated on Ficoll-Paque PLUS (GE Healthcare). Cells were stained with an antibody cocktail consisting of biotinylated anti-Gr-1, Mac-1, interleukin (IL)-7Rα, B220, CD4, CD8α, and Ter119 monoclonal antibodies. The monoclonal antibodies were purchased from eBioScience or BioLegend. Lineage-positive cells were depleted with goat anti-rat IgG microbeads (Miltenyi Biotec) through an LS column (Miltenyi Biotec). Cells were further stained with Alexa Fluor® 647 or eFluor® 660-conjugated anti-CD34, phycoerythrin (PE)-conjugated anti-Sca-1, and phycoerythrin/Cy7 (PE/Cy7)-conjugated anti-c-Kit antibodies. Biotinylated antibodies were detected with allophycocyanin/Cy7 (APC/Cy7)-conjugated streptavidin. Dead cells were eliminated by staining with Propidium iodide (1 μg/ml, Sigma). Analysis and sorting were performed on a FACS Aria II (BD Bioscience).

Cell Cycle Analysis

Fresh BM cells (1×10^7, CD45.2) were transplanted into 8-week-old CD45.1 mice irradiated at a dose of 9.5 Gy without competitor cells. Four months later, BM mononuclear cells were isolated on Ficoll-Paque PLUS. Cells were stained with an antibody cocktail consisting of biotinylated anti-Gr-1, Mac-1, IL-7Rα, B220, CD4, CD8α, Ter119, and CD45.1 monoclonal antibodies. Cells were further stained with Alexa Fluor® 700-conjugated anti-CD34, pacific blue-conjugated anti-Sca-1, and APC-conjugated anti-c-Kit antibodies. Biotinylated antibodies were detected with APC/Cy7-conjugated streptavidin. Analysis was performed on a FACS Aria II. To analyze the cell-cycle status, cells were incubated with 1 μg/ml Pyronin Y (Sigma) at 37°C for 45 min with protection from light. Bulk sorted $CD34^-LSK$ cells were incubated in SF-O3 supplemented with 50 μM?2-β-mercaptoethanol, 0.2% BSA, 1% GPS, 50 ng/ml SCF, 50 ng/ml TPO for 10 days at 37°C in a 5% CO_2 atmosphere. At day 10 of culture, the cell cycle profiles of culture cells were analyzed using an APC BrdU Flow Kit (BD Pharmingen). The cells were incubated with 10 μM BrdU at 37°C for 30 min and then stained with an antibody cocktail consisting of biotinylated anti-Gr-1,

Mac-1, IL-7Rα, B220, CD4, CD8α, and Ter119 monoclonal antibodies. Cells were further stained with PE-conjugated anti-Sca-1, and PE/Cy7-conjugated anti-c-Kit antibodies. Biotinylated antibodies were detected with APC/Cy7-conjugated streptavidin. Analysis was performed on a FACS Canto II (BD Bioscience).

Colony Assay

Colony assays were performed in methylcellulose-containing Iscove's modified Dulbecco's medium (Methocult M3234; Stemcell Technologies) supplemented with 20 ng/ml mouse SCF, 20 ng/ml mouse IL-3, 20 ng/ml human TPO, and 3 U/ml human EPO (Peprotech), and incubated at 37°C in a 5% CO_2 atmosphere. The number of HPP- and LPP-colony-forming cells (CFCs), which generate a colony with a diameter ≥1 mm and <1 mm, respectively, were evaluated by counting colonies at day 10–14 of culture. Colonies were individually collected, cytospun onto glass slides, and subjected to Hemacolor (MERCK) staining for morphological examination. To evaluate the proliferative and differentiation capacity of *Tie2-Cre;R26Stop^{FL}Bmi1* HSCs *in vitro*, single CD34$^-$LSK HSCs were clonally sorted into 96-microtiter plates containing 100 μl SF-O3 (Sanko Junyaku) supplemented with 50 μM 2-β-mercaptoethanol, 10% FBS, 1% L-glutamine, penicillin, streptomycin solution (GPS; Sigma), 10 ng/ml mouse SCF, 10 ng/ml human TPO, 10 ng/ml mouse IL-3, and 3 unit/ml human EPO (PeproTech). At day 14 of culture, the colonies were counted and individually collected for morphological examination. To evaluate the tolerance of test cells against oxidative stress, CD34$^-$LSK cells were cultured in the presence of DL-Buthionin-(*S,R*)-sulfoximine (BSO, Sigma) or *N*-Acetyl-L-cysteine (NAC, Sigma) for the indicated time periods, then subjected to colony assays or flow cytometric analyses.

Serial Transplantation and CRU Assays

Fresh BM cells (5×10^5, CD45.2) or 10-day cultured CD34$^-$LSK cells (CD45.2) corresponding to 20 initial CD34$^-$LSK cells were transplanted into 8-week-old recipient mice (CD45.1) irradiated at a dose of 9.5 Gy together with 5×10^5 and 2×10^5 BM competitor cells from 8-week-old CD45.1 mice, respectively. For serial transplantation, BM cells were collected from all recipient mice at 12–20 weeks after transplantation and pooled together. Then, 5×10^6 BM cells were transplanted into 8-week-old B6-CD45.1 mice irradiated at a dose of 9.5 Gy without competitor cells. Third and fourth transplantation were similarly performed using 5×10^6 pooled BM cells. Peripheral blood (PB) cells of the recipient mice were analyzed with a mixture of antibodies that included PE/Cy7-conjugated anti-CD45.1, pacific blue-conjugated anti-CD45.2, PE-conjugated anti-Mac-1 and anti-Gr-1, APC-conjugated anti-B220, and APC/Cy7-conjugated anti-CD4 and anti-CD8α antibodies. Cells were analyzed on a FACS Canto II. Percent donor chimerism was calculated as (% donor cells) ×100/(% donor cells + % recipient cells). To obtain the competitive repopulating units (CRUs), CRU assays were performed with a limiting number of test cells and the data were analyzed using L-Calc software (StemCell Technologies). Peripheral blood cell counts were made using an automated cell counter, Celltec α (Nihon Kohden).

Apoptosis Analysis

Bulk sorted CD34$^-$LSK cells were incubated in SF-O3 supplemented with 50 μM?2-β-mercaptoethanol, 0.2% BSA, 1% GPS, 50 ng/ml SCF, 50 ng/ml TPO for 10 days at 37°C in a 5% CO_2 atmosphere. At day 10 of culture, the cultured cells were incubated with APC-conjugated anti-Annexin V (BD Pharmingen) and propidium iodide at room temperature for 15 min with protection from light. Analysis was performed on FACS Canto II.

Immunostaining of γH2A.X

Cells were incubated in a culture medium drop on slide glasses pre-treated with poly-L-lysine (Sigma) for 2 hours. After fixation with 2% paraformaldehyde and blocking in 4% sheep serum for 30 min at room temperature, cells were incubated with purified anti-phospho-Histone H2A.X (Ser139) antibody (Cell Signaling Technology) for 12 hours at 4°C. The cells were then washed and incubated with Alexa Flour 555-conjugated anti-rabbit IgG goat polyclonal antibody (Invitrogen) for 60 min at room temperature. DNA was counterstained with 4′,6-diamidino-2-phenylindole (DAPI). Images were taken with a Keyence BZ-9000 fluorescence microscope.

RT-PCR

Total RNA was isolated using TRIZOL LS solution or TRIZOL solution (Invitrogen) and reverse transcribed by the ThermoScript RT-PCR system (Invitrogen) with an oligo-dT primer. Real-time quantitative polymerase chain reaction (PCR) was performed with an ABI prism 7300 Thermal Cycler (Applied Biosystems) using FastStart Universal Probe Master (Roche). The combination of primer sequences and probe numbers are as follows: for *p16^{Ink4a}*, probe #91, 5′-AATCTCCGCGAGGAAGC-3′, and 5′-GTCTGTCTGCAGCGGACTC-3′; for *p19^{Arf}*, probe #106, 5′-GGGTTTTCTTGGTGAAGTTCG-3′, 5′- TTGCCCATCATCATCACCT-3′, and for *Bmi1*, probe #95, 5′-AAACCAGACCACTCCTGAACA-3′ and 5′-TCTTCTTCTCTTCATCTCATTTTTGA-3′.

Western Blotting

Total cell lysate was resolved by SDS-PAGE and transferred to a PVDF membrane. The blots were probed with a mouse anti-Bmi1 (clone 8A9, kindly provided by Dr. N. Nozaki, MAB Institute, Co. Ltd., Japan), and a horseradish peroxidase-conjugated secondary antibody. The protein bands were detected with an enhanced chemiluminescence reagent (SuperSignal, Pierce Biotechnology).

Detection of ROS

Cells were stained with an antibody cocktail consisting of biotinylated anti-Gr-1, Mac-1, IL-7Rα, B220, CD4, CD8α, and Ter119 monoclonal antibodies. Cells were further stained with PE-conjugated anti-Sca-1, and PE/Cy7-conjugated anti-c-Kit antibodies. Biotinylated antibodies were detected with APC/Cy7-conjugated streptavidin. After staining with antibodies, cells were incubated with CellROX^{TM} Deep Red Reagent (5 μM, Invitrogen) at 37°C for 30 min with protection from light. Dead cells were eliminated by staining with propidium iodide (1 μg/ml, Sigma). Analysis was performed on a FACS Aria II.

Supporting Information

Figure S1 Steady state hematopoiesis in *Tie2-Cre;R26-StopFLBmi1* mice. (A) Hematopoietic analysis of 10-week-old *Tie2-Cre* and *Tie2-Cre;R26Stop^{FL}Bmi1* mice. Absolute numbers of CMPs, GMPs, MEPs, and CLPs in bilateral femurs and tibiae (upper panels), total spleen cells and LSK cells in the spleen (middle panel), and total thymic cells, CD4+CD8- cells, CD4-CD8+ cells, and CD4+CD8+ cells in the thymus (lower panels) are shown as the mean ± S.D. (*Tie2-Cre*; n = 8, *Tie2-Cre;R26-Stop^{FL}Bmi1*; n = 7). (B) Cell cycle status of CD34-LSK cells examined by Pyronin Y incorporation. Proportion of CD34-

LSK cells in the G0 phase of the cell cycle (Pyronin Y-) was shown as the mean ± S.D. (n = 4) (left panel). Representative flow cytometric profiles are also depicted (right panel).
(EPS)

Figure S2 Apoptosis and cell cycle status of *Tie2-Cre;R26Stop^{FL}Bmi1* LSK cells in culture. (A) The proportion of apoptotic cells in the LSK fraction in culture. CD34-LSK cells from *Tie2-Cre* (Control) and *Tie2-Cre;R26Stop^{FL}Bmi1* (Bmi1) mice were cultured in the SF-O3 serum-free medium supplemented with 50 ng/ml SCF and TPO. At day 10 of culture, apoptotic cells were detected by staining culture cells with anti-Annexin V and propidium iodide (PI). The percentage of Annexin V+PI- apoptotic cells in the LSK fraction is shown as the mean ± S.D. (n = 5). (B) The cell cycle status of LSK cells overexpressing Bmi1. CD34-LSK cells from *Tie2-Cre* (Control) and *Tie2-Cre;R26-Stop^{FL}Bmi1* (Bmi1) mice were cultured in the SF-O3 serum-free medium supplemented with 50 ng/ml SCF and TPO. At day 10 of culture, the cells were incubated with 10 μM BrdU at 37°C for 30 min and then analyzed using a BrdU Flow Kit. Data are shown as the mean ± SD (n = 4).
(EPS)

Figure S3 Hematopoietic recovery in recipients of *Tie2-Cre;R26Stop^{FL}Bmi1* HSCs after irradiation. Fresh BM cells from *Tie2-Cre* and *Tie2-Cre;R26Stop^{FL}Bmi1* mice (1×107, CD45.2) were transplanted into 8-week-old CD45.1 mice irradiated at a dose of 9.5 Gy without competitor cells. Four months later, the recipient mice were irradiated at a dose of 5 Gy. Changes in the PB cell count were monitored for 4 weeks (A) and the absolute number of BM LSK cells in bilateral femurs and tibiae was examined at 4 weeks post-irradiation (B). Data are shown as the mean ± SD (n = 5).
(EPS)

Figure S4 ROS levels in *Tie2-Cre;R26Stop^{FL}Bmi1* cells in culture. Levels of ROS in cells overexpressing Bmi1 in culture. CD34-LSK cells from *Tie2-Cre* (Control) and *Tie2-Cre;R26-Stop^{FL}Bmi1* (Bmi1) mice were cultured in the SF-O3 serum-free medium supplemented with 50 ng/ml SCF and TPO. Cells from day 11 or 12 of culture were further cultured for 2 days in the presence of 0.2 mM BSO, then levels of ROS in Lin-Sca-1+c-Kit+ cells and Lin-Sca-1low/−c-Kit+ cells were analyzed using CellROXTM Deep Red Reagent. Data are shown as dots and the mean values are indicated by bars (n = 4).
(EPS)

Acknowledgments

We thank Naohito Nozaki for the anti-Bmi1 antibody, George Wendt for critical reading of the manuscript, and Mieko Tanemura for laboratory assistance.

Author Contributions

Conceived and designed the experiments: SN AI. Performed the experiments: SN M. Oshima JY AS SM TK SY M. Osawa. Analyzed the data: SN AI. Contributed reagents/materials/analysis tools: HK HN. Wrote the paper: SN AI.

References

1. Simon JA, Kingston RE (2009) Mechanisms of polycomb gene silencing: knowns and unknowns. Nat Rev Mol Cell Biol 10: 697–708.
2. Iwama A, Oguro H, Negishi M, Kato Y, Nakauchi H (2005) Epigenetic regulation of hematopoietic stem cell self-renewal by polycomb group genes. Int J Hematol 81: 294–300.
3. Konuma T, Oguro H, Iwama A (2010) Role of the polycomb group proteins in hematopoietic stem cells. Dev Growth Differ 52: 505–516.
4. Sauvageau M, Sauvageau G (2010) Polycomb group proteins: multi-faceted regulators of somatic stem cells and cancer. Cell Stem Cell 7: 299–313.
5. Lessard J, Sauvageau G (2003) Bmi-1 determines the proliferative capacity of normal and leukaemic stem cells. Nature 423: 255–260.
6. Park IK, Qian D, Kiel M, Becker MW, Pihalja M, et al. (2003) Bmi-1 is required for maintenance of adult self-renewing haematopoietic stem cells. Nature 423: 302–305.
7. Iwama A, Oguro H, Negishi M, Kato Y, Morita Y, et al. (2004) Enhanced self-renewal of hematopoietic stem cells mediated by the polycomb gene product Bmi-1. Immunity 21: 843–851.
8. Oguro H, Iwama A, Morita Y, Kamijo T, van Lohuizen M, et al. (2006) Differential impact of Ink4a and Arf on hematopoietic stem cells and their bone marrow microenvironment in Bmi1-deficient mice. J Exp Med 203: 2247–2253.
9. Oguro H, Yuan J, Ichikawa H, Ikawa T, Yamazaki S, et al. (2010) Poised lineage specification in multipotent hematopoietic stem and progenitor cells by the polycomb protein Bmi1. Cell Stem Cell 6: 279–286.
10. Mihara K, Chowdhury M, Nakaju N, Hidani S, Ihara A, et al. (2006) Bmi-1 is useful as a novel molecular marker for predicting progression of myelodysplastic syndrome and patient prognosis. Blood 107: 305–308.
11. Rizo A, Horton SJ, Olthof S, Dontje B, Ausema A, et al. (2010) BMI1 collaborates with BCR-ABL in leukemic transformation of human CD34+ cells. Blood 116: 4621–4630.
12. Kisanuki YY, Hammer RE, Miyazaki J, Williams SC, Richardson JA, et al. (2001) Tie2-Cre transgenic mice: a new model for endothelial cell-lineage analysis in vivo. Dev Biol 230: 230–242.
13. Takano H, Ema H, Sudo K, Nakauchi H (2004) Asymmetric division and lineage commitment at the level of hematopoietic stem cells: inference from differentiation in daughter cell and granddaughter cell pairs. J Exp Med 199: 295–302.
14. Ema H, Takano H, Sudo K, Nakauchi H (2000) In vitro self-renewal division of hematopoietic stem cells. J Exp Med 192: 1281–1288.
15. Shima H, Takubo K, Iwasaki H, Yoshihara H, Gomei Y, et al. (2009) Reconstitution activity of hypoxic cultured human cord blood CD34-positive cells in NOG mice. Biochem Biophys Res Commun 378: 467–472.
16. Ito K, Hirao A, Arai F, Takubo K, Matsuoka S, et al. (2006) Reactive oxygen species act through p38 MAPK to limit the lifespan of hematopoietic stem cells. Nat Med 12: 446–451.
17. Yahata T, Takanashi T, Muguruma Y, Ibrahim AA, Matsuzawa H, et al. (2011) Accumulation of oxidative DNA damage restricts the self-renewal capacity of human hematopoietic stem cells. Blood 118: 2941–2950.
18. Rossi DJ, Jamieson CH, Weissman IL (2008) Stems cells and the pathways to aging and cancer. Cell 132: 681–696.
19. Chagraoui J, Hébert J, Girard S, Sauvageau G (2011) An anticlastogenic function for the Polycomb Group gene Bmi1. Proc Natl Acad Sci USA 108: 5284–5289.
20. Ginjala V, Nacerddine K, Kulkarni A, Oza J, Hill SJ, et al. (2011) BMI1 is recruited to DNA breaks and contributes to DNA damage-induced H2A ubiquitination and repair. Mol Cell Biol 31: 1972–1982.
21. Facchino S, Abdouh M, Chatoo W, Bernier G (2010) BMI1 confers radioresistance to normal and cancerous neural stem cells through recruitment of the DNA damage response machinery. J Neurosci 30: 10096–10111.
22. Shao L, Li H, Pazhanisamy SK, Meng A, Wang Y, et al. (2010) Reactive oxygen species and hematopoietic stem cell senescence. Int J Hematol 94: 24–32.
23. Jang YY, Sharkis SJ (2007) A low level of reactive oxygen species selects for primitive hematopoietic stem cells that may reside in the low-oxygenic niche. Blood 110: 3056–3063.
24. Liu J, Liu C, Chen J, Song S, Lee IH, et al. (2009) Bmi1 regulates mitochondrial function and the DNA damage response pathway. Nature 459: 387–392.
25. Rizo A, Olthof S, Han L, Vellenga E, de Haan G, et al. (2009) Repression of BMI1 in normal and leukemic human CD34$^+$ cells impairs self-renewal and induces apoptosis. Blood 114: 1498–1505.
26. Owusu-Ansah E, Banerjee U (2009) Reactive oxygen species prime Drosophila haematopoietic progenitors for differentiation. Nature 461: 537–541.
27. Bracken AP, Kleine-Kohlbrecher D, Dietrich N, Pasini D, Gargiulo G, et al. (2007) The polycomb group proteins bind throughout the INK4A-ARF locus and are disassociated in senescent cells. Genes Dev 21: 525–530.
28. Negishi M, Saraya A, Mochizuki S, Helin K, Koseki H, et al. (2010) A novel zinc finger protein Zfp277 mediates transcriptional repression of the Ink4a/Arf locus through polycomb repressive complex 1. PLoS One 5: e12373.
29. Kamminga LM, Bystrykh LV, de Boer A, Houwer S, Douma J, et al. (2006) The Polycomb group gene Ezh2 prevents hematopoietic stem cell exhaustion. Blood 107: 2170–2179.
30. Stapels M, Piper C, Yang T, Li M, Stowell C, et al. (2010) Polycomb group proteins as epigenetic mediators of neuroprotection in ischemic tolerance. Sci Signal 3: ra15.
31. Bracken AP, Helin K (2009) Polycomb group proteins: navigators of lineage pathways led astray in cancer. Nat Rev Cancer 9: 773–784.

32. Diehn M, Cho RW, Lobo NA, Kalisky T, Dorie MJ, et al. (2009) Association of reactive oxygen species levels and radioresistance in cancer stem cells. Nature 458: 780–783.
33. Zhou J, Bi C, Cheong LL, Mahara S, Liu SC, et al. (2011) The histone methyltransferase inhibitor, DZNep, up-regulates TXNIP, increases ROS production, and targets leukemia cells in AML. Blood 118: 2830–2839.
34. Sasaki Y, Derudder E, Hobeika E, Pelanda R, Reth M, et al. (2006) Canonical NF-kappaB activity, dispensable for B cell development, replaces BAFF-receptor signals and promotes B cell proliferation upon activation. Immunity 24: 729–739.
35. Fukamachi H, Fukuda K, Suzuki M, Furumoto T, Ichinose M, et al. (2001) Mesenchymal transcription factor Fkh6 is essential for the development and differentiation of parietal cells. Biochem Biophys Res Commun 280: 1069–1076.

blood

2012 119: 6234-6242
Prepublished online May 16, 2012;
doi:10.1182/blood-2011-07-367441

Generation of induced pluripotent stem cells from primary chronic myelogenous leukemia patient samples

Keiki Kumano, Shunya Arai, Masataka Hosoi, Kazuki Taoka, Naoya Takayama, Makoto Otsu, Genta Nagae, Koki Ueda, Kumi Nakazaki, Yasuhiko Kamikubo, Koji Eto, Hiroyuki Aburatani, Hiromitsu Nakauchi and Mineo Kurokawa

Blood (print ISSN 0006-4971, online ISSN 1528-0020), is published weekly by the American Society of Hematology, 2021 L St, NW, Suite 900, Washington DC 20036.

Generation of induced pluripotent stem cells from primary chronic myelogenous leukemia patient samples

Keiki Kumano,[1,2] Shunya Arai,[1,2] Masataka Hosoi,[1,2] Kazuki Taoka,[1,2] Naoya Takayama,[3,4] Makoto Otsu,[5] Genta Nagae,[6] Koki Ueda,[1,2] Kumi Nakazaki,[1,2] Yasuhiko Kamikubo,[1,2] Koji Eto,[3,4] Hiroyuki Aburatani,[6] Hiromitsu Nakauchi,[3,5] and Mineo Kurokawa[1,2]

[1]Department of Hematology and Oncology, Graduate School of Medicine, University of Tokyo, Tokyo, Japan; [2]Core Research for Evolutional Science and Technology, Japan Science and Technology Agency, Tokyo, Japan; [3]Stem Cell Bank, Center for Stem Cell Biology and Regenerative Medicine, Institute of Medical Science, University of Tokyo, Tokyo, Japan; [4]Center for iPS Cell Research and Application, University of Kyoto, Kyoto, Japan; [5]Division of Stem Cell Therapy, Center for Stem Cell Biology and Regenerative Medicine, Institute of Medical Science, University of Tokyo, Tokyo, Japan; and [6]Genome Science Division, Research Center for Advanced Science and Technology, University of Tokyo, Tokyo, Japan

Induced pluripotent stem cells (iPSCs) can be generated by the expression of defined transcription factors not only from normal tissue, but also from malignant cells. Cancer-derived iPSCs are expected to provide a novel experimental opportunity to establish the disease model. We generated iPSCs from imatinib-sensitive chronic myelogenous leukemia (CML) patient samples. Remarkably, the CML-iPSCs were resistant to imatinib although they consistently expressed BCR-ABL oncoprotein. In CML-iPSCs, the phosphorylation of ERK1/2, AKT, and JNK, which are essential for the maintenance of both BCR-ABL (+) leukemia cells and iPSCs, were unchanged after imatinib treatment, whereas the phosphorylation of signal transducer and activator of transcription (STAT)5 and CRKL was significantly decreased. These results suggest that the signaling for iPSCs maintenance compensates for the inhibition of BCR-ABL. CML-iPSC–derived hematopoietic cells recovered the sensitivity to imatinib although $CD34^{+}38^{-}90^{+}45^{+}$ immature cells were resistant to imatinib, which recapitulated the pathophysiologic feature of the initial CML. CML-iPSCs provide us with a novel platform to investigate CML pathogenesis on the basis of patient-derived samples. (*Blood*. 2012;119(26):6234-6242)

Introduction

Hematologic malignancies including leukemias are often chemotherapy-resistant, most of which follows an aggressive clinical course.[1] Multiple drug therapies are usually required to treat them, although they are occasionally accompanied with many side effects. Thus, the invention of novel targeted therapies based on newly revealed molecular pathogenesis is expected to overcome the current situation.[2] However, previous approaches to understanding pathogenesis involve several limitations. Many mouse models of human diseases have been established, but they may not fully recapitulate many aspects of original human diseases.[3] Many kinds of cell lines are also available for research. However, they do not cover all diseases, because it is usually difficult to establish a cell line from a primary patient sample. Furthermore, additional gene mutations may be accumulated in cell lines. Theoretically, primary patient samples should be used for research, but the amount of obtained cells may be inadequate for various analyses.

Induced pluripotent stem cells (iPSCs) can be generated from various types of cells by the transduction of defined transcription factors.[4-10] In addition to the regenerative medicine,[11] iPSCs have been used for studies of the pathogenesis of inherited genetic diseases.[12-16] Recently, it was reported that iPSCs were generated not only from normal tissue cells, but also from malignant cells.[17-20] In those cases, cancer cells themselves must have been the origins of iPSCs. However, in most published data, established cell lines were used as the source material of cancer cells, including chronic myelogenous leukemia (CML),[17] gastrointestinal cancers,[18] and melanoma,[19] except for the JAK2-V617F mutation (+) polycythemia vera (PV) patient.[20]

CML is a myeloproliferative neoplasm that originates from hematopoietic stem cells transformed by the *BCR-ABL* fusion gene. The initial indolent chronic phase (CP) is followed by aggressive stages, the accelerated phase (AP), and the blast crisis (BC), in which immature leukemic cells expand.[21] CML is now initially treated with one of several tyrosine kinase inhibitors (TKIs) including imatinib, dasatinib, and nilotinib, which have dramatically improved the long-term survival rate of CML patients up to approximately 90%. However, even TKIs are not able to eradicate the CML clone completely, which is demonstrated by the fact that discontinuation of TKIs in molecular remission CML patients usually leads to the recurrence of the BCL-ABL clone. Therefore, many studies are performed to elucidate the mechanisms of TKI-resistance in CML stem cells and to overcome the resistance.

In this study, we established iPSCs from primary CML patient samples, redifferentiated them into hematopoietic lineage and showed the recapitulation of the pathophysiologic features of the initial disease.

Submitted July 14, 2011; accepted April 30, 2012. Prepublished online as *Blood* First Edition paper, May 16, 2012; DOI 10.1182/blood-2011-07-367441.

The online version of this article contains a data supplement.

The publication costs of this article were defrayed in part by page charge payment. Therefore, and solely to indicate this fact, this article is hereby marked "advertisement" in accordance with 18 USC section 1734.

Methods

Cell and cell culture

Primary samples of CML bone marrow cells were obtained after informed consent. All studies using human cells were reviewed and approved by the institutional review boards (IRBs) of University of Tokyo. Mononuclear cells (MNCs) were isolated by centrifugation through a Ficoll gradient. $CD34^+$ cells were isolated by an immunomagnetic separation technique (auto magnetic-activated cell sorting; MACS). They were cultured with α-minimum essential medium (MEM) containing 20% fetal calf serum (FCS) supplemented with 100 ng/mL stem cell factor (SCF; Wako), 10 ng/mL thrombopoietin (TPO; Wako), 100 ng/mL FL3L (Wako), 10 ng/mL IL3 (Wako), and 100 ng/mL IL6 (Wako).

Normal iPSCs established from cord blood (CB) $CD34^+$ cells or fibroblasts[22] and CML-iPSCs were maintained in Dulbecco modified Eagle medium-F12 (Invitrogen) supplemented with 20% knockout serum replacement (KSR; Invitrogen), 0.1mM 2-mercaptoethanol (Sigma-Aldrich), MEM nonessential amino acids (Invitrogen), and 5 ng/mL recombinant human basic fibroblast growth factor (FGF; Peprotech) on mitomycin C (MMC)–treated mouse embryo fibroblast (MEF) feeder cells.[23] Imatinib (LC Laboratories) was added to the culture medium at the various concentrations (1-10μM). U0126 and LY294004 (LC Laboratories) were used to inhibit ERK and AKT, respectively.

The mouse C3H10T1/2 cells were cultured as previously described.[24]

Production of VSV-G pseudotyped retroviral particles

Construction of pMXs vectors encoding Oct3/4, Sox2, Klf4, and c-myc were performed as previously described.[22] Highly concentrated VSV-G–pseudotyped retroviral supernatant was prepared using reported procedures. The 293GPG cells were kind gifts from Dr R. C. Mulligan (Children's Hospital Boston, Harvard Medical School, Boston, MA).[25] Stable 293GPG cell lines, each capable of producing VSV-G–pseudotyped retroviral particles on induction were established as previously described.[22,25] Retroviral supernatants were concentrated by centrifugation for 16 hours at 6000*g*.

Generation of iPSCs from CML samples

Two days before infection, cells were stimulated with cytokines as mentioned in "Cell and cell culture." For infection, each well of a 24-well dish coated with a fibronectin fragment CH296:RetroNectin (Takara-Bio) was covered with virus-containing supernatants. After the adhesion of viruses according to the manufacture's recommendation, 1×10^5 cells of $CD34^+$ CML cells or CB cells were inoculated into each well and filled with the culture medium supplemented with cytokines. The next day, concentrated viral supernatant was added to the culture. On day 3 after infection, cells were harvested with vigorous pipetting, washed by phosphate-buffered saline (PBS), and cultured with the same fresh medium for next 3 days. On day 6, cells were seeded on MMC treated MEF cells. Two to 4 days after, the medium was replaced with human ES medium as previously described with 0.5mM valproic acid (VPA; Sigma-Aldrich).[26] Subsequently, medium was changed every other day. After 20 days, ES-like colonies appeared. Using live cell imaging technology with Tra-1-60 antibody as previously described,[27] each fully reprogrammed colony was distinguished from deficiently reprogrammed colonies, and was picked up to be reseeded on new MEF feeder cells. Cloned ES-like colonies were subjected to further analysis.

Antibodies, FACS analysis, and immunocytochemistry

The following fluorescent conjugated antibodies were used for fluorescence-activated cell sorter (FACS) analysis and immunocytochemistry: anti–human stage specific embryonic antigen (SSEA)–4 conjugated with Alexa Fluor 488 (BD Bioscience), anti–human tumor related antigen (TRA)–1-60 conjugated with Alexa Fluor 555 (BD Bioscience), anti-CD34 phycoerythrin (PE) conjugated (Beckman Coulter), and anti-CD45 fluorescein isothiocyanate (FITC) conjugated (Beckman Coulter).

Cells were sorted with a FACSAria, and analysis was performed on FACS LSRII (BD Bioscience).

For immunocytochemistry, cells were fixed with 4% paraformaldehyde in PBS, after which they were labeled with an antibody against human SSEA-4 and antibody against human TRA-1-60 antibody and observed using a confocal microscope (Carl Zeiss).

Methylation profiling

Genomic DNA was extracted using the QIAamp DNA Mini Kit (QIAGEN) according to the manufacture's instruction. Methylation status was evaluated as previously reported.[28] Methylation status was analyzed using HumanMethylation27 BeadChip (Illumina). Genomic DNA for methylation profiling was quantified using the Quant-iT dsDNA BR assay kit (Invitrogen). Five-hundred nanograms of genomic DNA was bisulfite-converted using an EZ DNA methylation kit (Zymo Research). The converted DNA was amplified, fragmented and hybridized to a beadchip according to the manufacturer's instructions. The raw signal intensity for both methylated (M) and unmethylated (U) DNA was measured using a BeadArray Scanner (Illumina). The methylation level of the each individual CpG is obtained using the formula (M)/(M) + (U) + 100 by the GenomeStudio (Illumina).

Microarray analysis

Gene expression analysis was carried out as previously described[29] with the use of the Human Genome U133 Plus 2.0 Array (Affymetrix). The hierarchical clustering techniques classify data by similarity and their results are represented by dendrograms. Previously reported data of human embryonic stem (ES) cells (GSM449729) and CML $CD34^+$ cells (GSM366215, 366216, 366221, and 366222) were used to compare the gene expression profile. The microarray data are available on the Gene Expression Omnibus (GEO) database under accession number GSE37982.

Hematopoietic differentiation of iPSCs

To differentiate iPSCs into hematopoietic cells, we used the same protocol previously used with ES cells and iPSCs.[22,24] In brief, small clusters of iPSCs (< 100 cells treated with PBS containing 0.25% trypsin, 1mM $CaCl_2$, and 20% KSR) were transferred onto irradiated 10T1/2 cells and cocultured in hematopoietic cell differentiation medium, which was refreshed every third day. Differentiation medium consists of Iscove modified Dulbecco medium supplemented with a cocktail of 10 μg/mL human insulin, 5.5 μg/mL human transferrin, 5 ng/mL sodium selenite, 2mM L-glutamine, 0.45mM α-monothioglycerol, 50 μg/mL ascorbic acid, and 15% highly filtered FBS in the presence of 20 ng/mL human vascular endothelial growth factor (VEGF).[24] On days 14 to 15 of culture, the iPS-sacs were collected into a 50-mL tube, gently crushed with a pipette tip and passed through a 40-μm cell strainer to obtain hematopoietic progenitors. Hematopoietic progenitors were collected by sorting with CD34 and CD45 antibodies, Giemsa stained, and then examied under a microscope. Hematopoietic progenitors were cultured in the α-medium plus 20% FCS supplemented with 100 ng/mL SCF, 10 ng/mL TPO, 100 ng/mL FL3L, 10 ng/mL IL3, and 100 ng/mL IL6.

Hematopoietic colony-forming cell (CFC) assay

CFC assays were performed in MethoCult H4434 semisolid medium (StemCell Technologies). Ten thousand hematopoietic progenitors harvested from an iPS-Sacs were plated in 1.5 mL of medium and cultivated for 14 days.

RT-PCR and quantitative real-time PCR analysis

After extraction of total RNA with RNAeasy reagents (QIAGEN), reverse transcription was performed with SuperScript III (Invitrogen). Primer

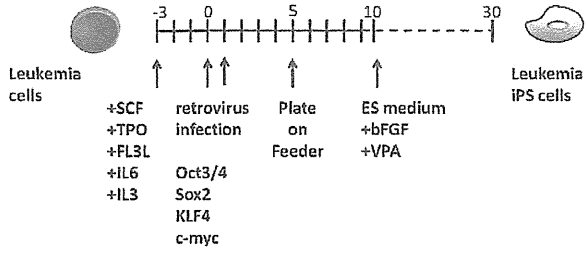

Figure 1. Experimental scheme for generating of iPSCs from the CML patient sample. After cytokine stimulation, $CD34^+$ CML cells were reprogrammed by transduction with Yamanaka factors. To improve the reprogramming, valproic acid was added to the culture.

sequences used for the detection of stem cell genes were as previously described.[9]

Quantitative real-time PCRs (qPCRs) were carried out in the ABI-7000 sequence detection system with SYBR Green PCR Core reagents according to the manufacturer's instructions (Applied Biosystems). We analyzed expression levels of *BCR-ABL* fusion transcript as previously described.[30] Each assay was performed in triplicate and the results were normalized to GAPDH (glyceraldehyde-3-phosphate dehydrogenase) levels.

PCR primers used for quantitative PCR:
BCR-ABL F TCAGAAGCTTCTCCCTGACATCCGT
BCR-ABL R TCCACTGGCCACAAAATCATACAGT
GAPDH F TGCACCACCAACTGCTTAGC
GAPDH R GGCATGGACTGTGGTCATGAG

Western blotting

Fifty micrograms of cell lysates were subjected to sodium dodecylsulfate-polyacrylamide gel electrophoresis (SDS-PAGE) and Western blot analysis. Antibodies used in immunoblotting were as follows; anti-phospho ERK1/2 (Thr202/Tyr204; Cell Signaling), anti-phospho Akt (Ser473; Cell Signaling), anti-phospho JNK (Thr183/Tyr185; Cell Signaling), anti-phospho-STAT5 (Tyr694; Cell Signaling), and anti-phospho CRKL (Tyr207; Cell Signaling). Enhanced chemiluminescence detection (Amersham) was carried out according to the manufacturer's recommendations.

Results

Generation of iPSCs from primary CML patient samples

After obtaining informed consent, $CD34^+$ cells were purified from bone marrow mononuclear cells of a CML chronic phase patient. After we stimulated them with cytokines for 2 days, retroviral transduction with the transcription factors OCT3/4, SOX2, KLF4, and MYC was performed. Two days after transduction, we reseeded cells onto MEF cells and cultured them for another 2 days. Then, we replaced the medium with human ES medium supplemented with 5 ng/mL bFGF. To improve the efficiency of the reprogramming, we added VPA,[26] a histone deacetylase inhibitor, to the culture (Figure 1). Using a live cell imaging method with Tra-1-60 antibody, bona fide iPSCs were distinguished from deficiently reprogrammed cells.[27] As a result, 2 CML-derived iPSCs (CML-iPSCs) were generated, which were derived from independent patients. CML-iPSCs showed the typical morphology as iPSCs (Figure 2A) and expressed the pluripotency markers, such as SSEA-4 and Tra-1-60 (Figure 2B), and the endogenous expression of embryonic stem cell (ESC) characteristic transcripts (OCT3/4, SOX2, KLF4, NANOG, LIN28, and REX1) was confirmed by RT-PCR (Figure 2C). CML-iPSCs also expressed BCR-ABL, which demonstrated that they were truly derived from CML (Figure 2D). Furthermore, fluorescence in situ hybridization with dual color *BCR-ABL* probes confirmed t(9;22) translocation in CML-iPSCs at the single cell level (supplemental Figure 1A and supplemental Table 1, available on the *Blood* Web site; see the Supplemental Materials link at the top of the online article). However, although CML-iPSCs expressed BCR-ABL, they were resistant to imatinib (Figure 2E). Teratoma formation capacity was confirmed, demonstrating the pluripotency of CML-iPSCs (supplemental Figure 2).

Comprehensive analysis of DNA methylation revealed that methylation pattern of CML-iPSCs was different from that of original CML sample but was very similar to that of normal iPSCs although there were slight differences (Figure 3A). Previously, stem cell–specific differentially methylated regions (SS DMRs)

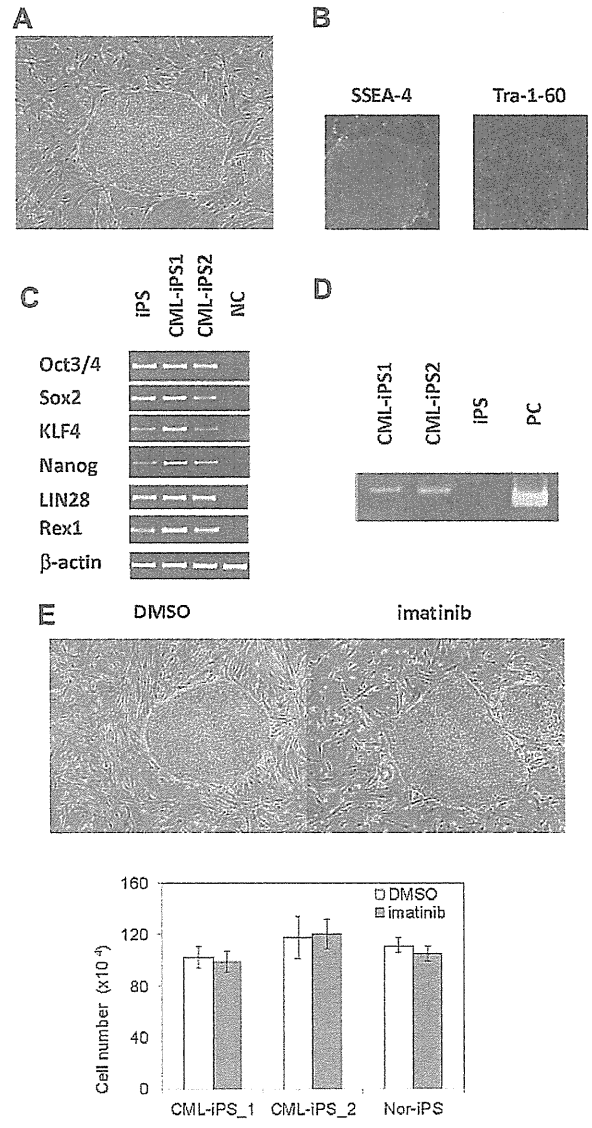

Figure 2. Generation of CML derived iPSCs. (A) Morphology of CML-iPSCs. (B) Immunofluiorescence staining shows expression of pluripotent marker (left: SSEA-4 and right: Tra-1-60) in CML-iPSCs. (C) RT-PCR analysis of ES cell marker genes. Endogenous expression of these stem cell–specific genes in CML-iPSCs was verified. (D) CML-iPSCs expressed the BCR-ABL fusion transcript. (E) Imatinib (10μM) were added to the culture of iPSCs. DMSO (top left panel) and imatinib (top right panel) treated CML-iPSCs were shown. The number of alive CML-iPSCs (CML-iPS_1 and CML-iPS_2) and normal iPSCs (Nor-iPS) after 5 days treatment was calculated (bottom panel). These were the representative data from 3 independent experiments.

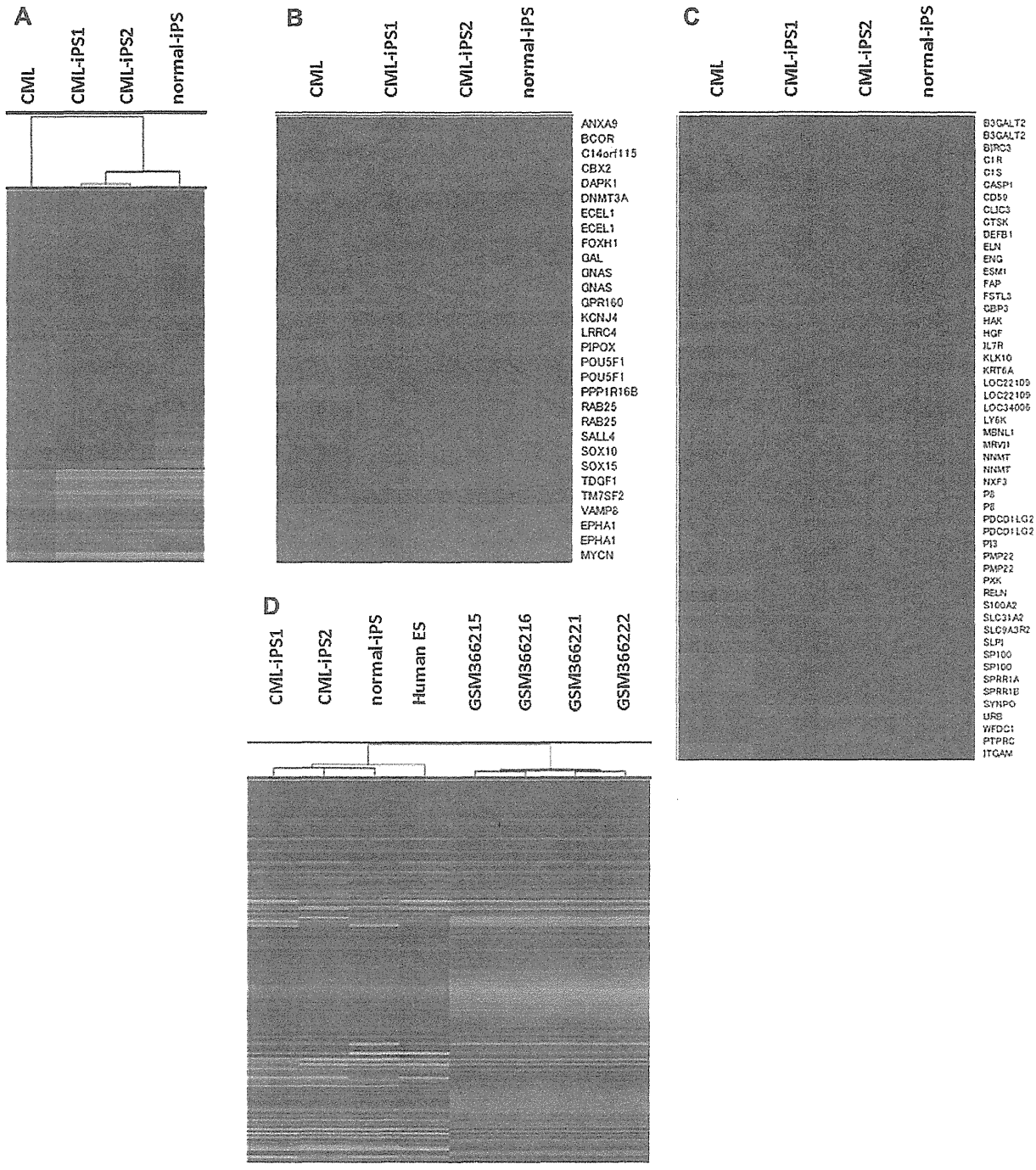

Figure 3. Comprehensive analysis of DNA methylation and gene expression. (A) Unsupervised hierarchical clustering based on differentially methylated CpGs is shown on the dendrogram. The accompanying heatmap shows the methylation status across 5001 differentially methylated CpGs. In the heatmap, red indicates a CpG methylation more than 50%, and green less than 50%. The methylation status in hypo SS DMRs (B) or hyper SS DMRs (C) was shown in the heatmap. (D) Unsupervised hierarchical clustering based on global gene expression data are shown on the dendrogram. The accompanying heatmap shows the normalized log2 transformed expression values (Z-scores) for each probe. In the heatmap, red indicates expression more than mean, and green less than mean.

were identified during reprogramming process of iPSCs.[31] Hypomethylated SS DMRs (hypo SS DMRs) in the variety of iPSCs were also hypomethylated in the CML-iPSCs including the promoters of OCT4 (Figure 3B). In the same way, hypermethylated SS DMRs (hyper SS DMRs) in the variety of iPSCs were also hypermethylated in the CML-iPSCs (Figure 3C). The promoters of hematopoietic lineage-specific marker genes, such as CD45 and CD11b, were hypermethylated in the CML-iPSCs. Thus, the methylation pattern of CML-iPSCs was confirmed to be not hematopoietic cell-like, but iPSC-like. Next, we compared the gene expression pattern among CML-iPSCs and normal iPSCs (Figure 3D). In a result, CML-iPSCs and normal iPSCs were very similar in regard to global gene expression profile. Furthermore, comparing our results with publicly available expression data of human ES cells and CML $CD34^+$ cells, we found that CML-iPSCs were very similar to human ES cells, whereas they were different

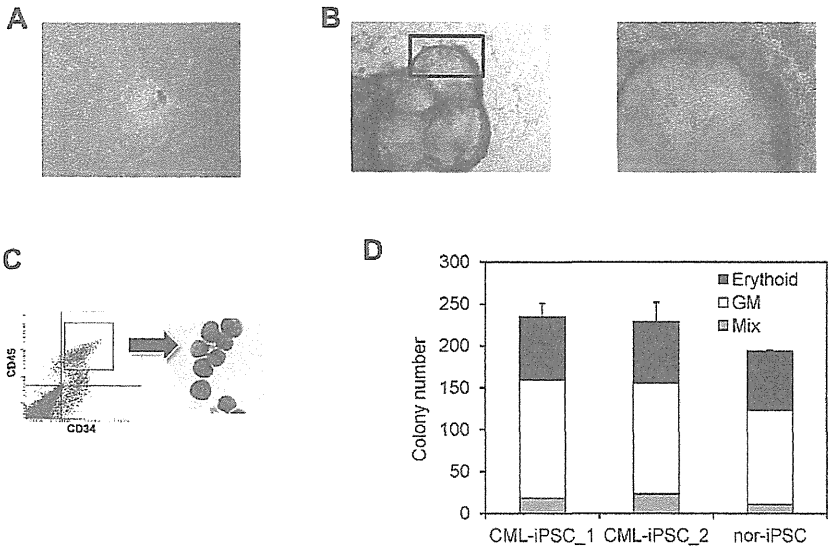

Figure 4. Hematopoietic differentiation of CML-iPSCs. CML-iPSCs were differentiated on the 10T1/2 cells. On day 7 (A), iPSCs began to mount. On day 14 of culture (B: left panel), inflated sac-like structures appeared. These sac-like structures contained the round hematopoietic cells (B: right panel: higher magnification). (C) These hematopoietic cells expressed immature marker CD34 and CD45. (D) CFC activity was estimated using 1×10^4 $3CD34^+$ $CD45^+$cells. Erythroid colonies (black bars), granulocyte-monocyte (GM) colonies (white bars), and mixed GM colonies with erythtoid cells (mix; gray bars) were plotted.

from CML $CD34^+$ cells in terms of gene expression patterns (Figure 3D).

Hematopoietic differentiation of CML-iPSCs

Then we differentiated them into hematopoietic progenitors within the "unique sac-like structures" (iPS-sacs; Figure 4A-B). This method was reported to be able to produce the hematopoietic progenitors with higher efficiency than the usual embryoid body formation method using human ESCs and iPSCs.[22,24] On day 15 of culture, iPSCs sacs contained round hematopoietic-like cells (Figure 4B). Then we picked up iPS-sacs with a pipette tip and dissociated them mechanically and obtained the inner round cells. Round cells, positive for a hematopoietic lineage marker CD45 and an immature marker CD34, proved to be hematopoietic progenitors (Figure 4C).

Then we characterized the CML-iPSCs derived hematopoietic cells, comparing with those derived from normal iPSCs. CFC activities were measured using the same number of $CD34^+$ cells (Figure 4D). Hematopoietic progenitors derived from CML-iPSCs and normal iPSCs produced colonies of mature erythroid, granulocyte-macrophage, or mixed of these hematopoietic cells in growth factor-supplemented methyl cellulose medium with a similar distribution of colony size, morphologies, and kinetics of growth and maturation. The colony forming cells expressed BCR-ABL (supplemental Figure 1B and supplemental Table 2).

Next, we tested the engraftment potential of these cells. nonobese diabetic/severe combined immunodeficiency IL2Rg deficient (NOG) mice serve as a superior host for engraftment of human normal and malignant hematopoietic cells.[32] One million $CD34^+$ cells were intravenously transplanted into NOG mice with minimal irradiation (2 Gy; supplemental Figure 3A). Only transient engraftment was observed and the recipient mice never showed CML phenotype in vivo (supplemental Figure 3B).

BCR-ABL dependence is lost in the CML-iPSCs

The restricted dependence of BCR-ABL signaling on survival of CML cells enables the disease suppression by imatinib and dramatically changed the CML treatment after the development of imatinib.[33] CML patients whose cells were used for the generation of iPSCs effectively responded to imatinib therapy. However, although CML-iPSCs expressed BCR-ABL, they were resistant to imatinib (Figure 2E). Interestingly, CML-iPSC–derived hematopoietic cells recovered the sensitivity to imatinib except $CD34^+38^-90^+45^+$ immature cell population, which recapitulated the feature of initial CML disease (Figure 5A). Various concentrations of imatinib were added to the culture of iPSC derived hematopoietic cells. Similar kinetics of imatinib response between CML-iPSC–derived hematopoietic cells and imatinib sensitive CML cell line K562 was observed (Figure 5B). Furthermore, we generated $CD34^+CD38^-CD90^+CD45^+$ cells from CML-iPSCs. Surprisingly, this fraction of phenotypically immature cells showed the imatinib resistance like CML-iPSCs although more differentiated cells ($CD34^-CD45^+$) showed the sensitivity to imatinib (Figure 5C).

Then, we investigated why CML-iPSCs showed the imatinib-resistance. It was reported that imatinib resistant patients sometimes express higher BCR-ABL transcript than imatinib sensitive patients.[34] In addition, CML leukemia stem cells showed higher BCR-ABL expression than differentiated CML cells.[35] Therefore, we examined the BCR-ABL mRNA expression levels in the CML-iPSCs, and compared them with the primary CML sample, and CML-iPSC–derived hematopoietic cells. As a result, BCR-ABL expression was not increased in CML-iPSCs compared with the primary CML sample and CML-iPSCs–derived hematopoietic cells. (Figure 6A)

BCR-ABL activates Ras-MAPK, PI3K-AKT, JAK-STAT pathways. Among them, it was reported that STAT5, ERK1/2, JNK, and AKT are essential for the survival of BCR-ABL–dependent leukemic cells.[36,37] In addition, CRKL is another direct target of BCR-ABL.[38] The phosphorylation status of ERK1/2, AKT, JNK, and STAT5 in CML-iPSCs, which are essential for the survival of BCR-ABL (+) hematopoietic progenitors, were evaluated after imatinib treatment. The phosphorylation of ERK1/2, AKT, and JNK, which are also essential for the maintenance of iPSCs and ES cells,[39,40] were unchanged after treatment in the CML-iPSCs although they were decreased in the CML-iPSCs–derived hematopoietic cells (Figure 6B). The phosphorylation of CRKL and STAT5, which were not activated in the normal iPSCs, was decreased in both CML-iPSCs and CML-iPSCs–derived hematopoietic cells (Figure 6B). These results showed that the signaling for iPSCs maintenance

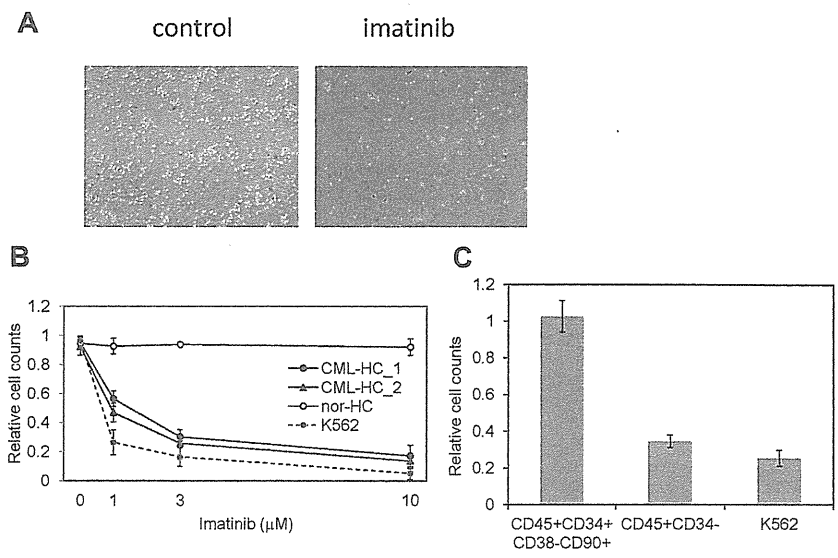

Figure 5. CML-iPSC derived hematopoietic cells recovered the sensitivity to imatinib. (A) Imatinib but not the vehicle (DMSO) decreased the growth of hematopoietic cells derived from CML-iPSCs in suspension culture. (B) Various concentrations of imatinib were added to the culture of iPSC derived hematopoietic cells for 4 days. CML-iPSC–derived $CD34^+$ hematopoietic cells (CML-HC_1 and CML-HC_2), normal iPSC-derived hematopoietic cells (nor-HC), and K562 cells were used for analyses. Relative cell counts compared with the vehicle control were plotted. Shown is the mean of a single experiment conducted in triplicate as a representative of 3 independent experiments. (C) Imatinib (10μM) was added to the suspension culture of CML-iPSC–derived hematopoietic cells for 4 days. The immature cell fraction ($CD34^+CD38^-CD90^+CD45^+$) showed resistance similar to CML-iPSCs, although more differentiated cells ($CD34^-CD45^+$) showed the sensitivity to imatinib. Relative cell counts compared with the vehicle control was plotted.

might compensate for the inhibition of BCR-ABL in CML-iPSCs and that BCR-ABL dependence was lost in CML-iPSCs. In addition, the specific inhibitor of ERK or AKT signaling worked as expected, respectively (Figure 6C), resulting in the reduction of attached cells regardless of the addition of imatinib (Figure 6D).

Discussion

Generation of CML-derived iPSCs

We generated iPSCs from primary CML patient samples. Methylation pattern and gene expression of CML-iPSCs were very similar to those of normal iPSCs. Previously, SS DMRs were identified during reprogramming process of iPSCs.[31] Hypo SS DMRs were also hypomethylated in the CML-iPSCs (Figure 3B). Among them, some genomic regions, such as the promoter of N-MYC, had already been hypomethylated in the primary CML sample. In the same way, some genes associated with hyper SS DMRs had already been hypermethylated in the primary CML sample (Figure 3C). However, we could not detect the CML-iPSC–specific DMRs in this study. Then, we redifferentiated them into hematopoietic lineage and showed the recapitulation of the features of the initial disease. In addition, although CML-iPSCs expressed BCR-ABL, it was surprising that there were no obvious differences of gene expression profile between normal iPSCs and CML-iPSCs (Figure 3D). The results that inhibition of BCR-ABL by imatinib did not affect CML-iPSC survival indicate that signaling of BCR-ABL might not be important in iPSCs. These results are consistent with the gene expression profile data in which the effect of BCR-ABL signaling was hardly observed. One possibility is that global tyrosine kinase activities and downstream signaling pathways would be so activated in iPSCs irrespective of BCR-ABL that BCR-ABL no longer adds significant effects.

CML is known to be a clonal disorder originated from hematopoietic stem cells caused by BCR-ABL fusion gene. Although BCR-ABL TKI imatinib can reduce CML cells below the detection of molecular level, its discontinuation often results in the rapid relapse of leukemia.[41] These results indicate the existence of CML stem cells, which are resistant to the TKI. CML stem cells are thought to be included in the primitive population ($CD34^+CD38^-$). According to some published data, they have lost the addiction to BCR-ABL[42,43] In addition, CML-iPSCs also have shown resistance to the imatinib.[44] Furthermore, in our experiments, immature $CD34^+38^-90^+45^+$ cells differentiated from CML-iPSCs also showed imatinib resistance similar to CML-iPSCs, although more differentiated cells ($CD34^-CD45^+$) showed sensitivity to imatinib (Figure 5C). So, these immature cells showed a phenotype of CML stem cells. Imatinib treatment of CML stem cells decreased the phosphorylation of CRKL and STAT5 but not of AKT,[42] as shown in the CML-iPSCs described here. There may be some shared mechanism between CML stem cells and CML-iPSCs. For example, Wnt-β-catenin signaling is essential for the maintenance of both CML stem cells and iPSCs.[45,46] Using immature cells obtained in our study, the mechanism of imatinib resistance of CML stem cells can be further investigated.

Previously, it was reported that primary CML samples and the CML BC cell line KBM7 were reprogrammed and that primary CML-iPSCs[47] and KBM7-iPSCs were established.[17] As shown here, KBM7-iPSCs lost the BCR-ABL dependence and became resistant to imatinib, although primary CML-derived iPSCs were not checked for the imatinib sensitivity. Carette et al argued that a specific differentiated epigenetic cell state is needed to maintain BCR-ABL dependence.[17] However, they only showed the BCR-ABL expression but did not confirm BCR-ABL activation in the KBM7-iPSCs. We showed BCR-ABL specific phosphorylation of STAT5 and CRKL although they were not necessary for the survival of iPSCs and that imatinib treatment inhibits these signaling. On the other hand, RAS-MAPK and PI3K-AKT signaling were unchanged after imatinib treatment. It was reported that inhibition of caspase-mediated anoikis by bFGF is dependent on activation of ERK and AKT in human ES cells.[39] We also showed that the inhibition of ERK or AKT irrespective of the presence of the imatinib resulted in the decrease of the attached cell numbers. Some key molecules essential for the maintenance of iPSCs may compensate for the BCR-ABL inhibition in the CML-iPSCs through downstream ERK and AKT signaling pathways. They may include contact-mediated signaling with stem cell niches, and may be shared with CML stem cells and CML-iPSCs.

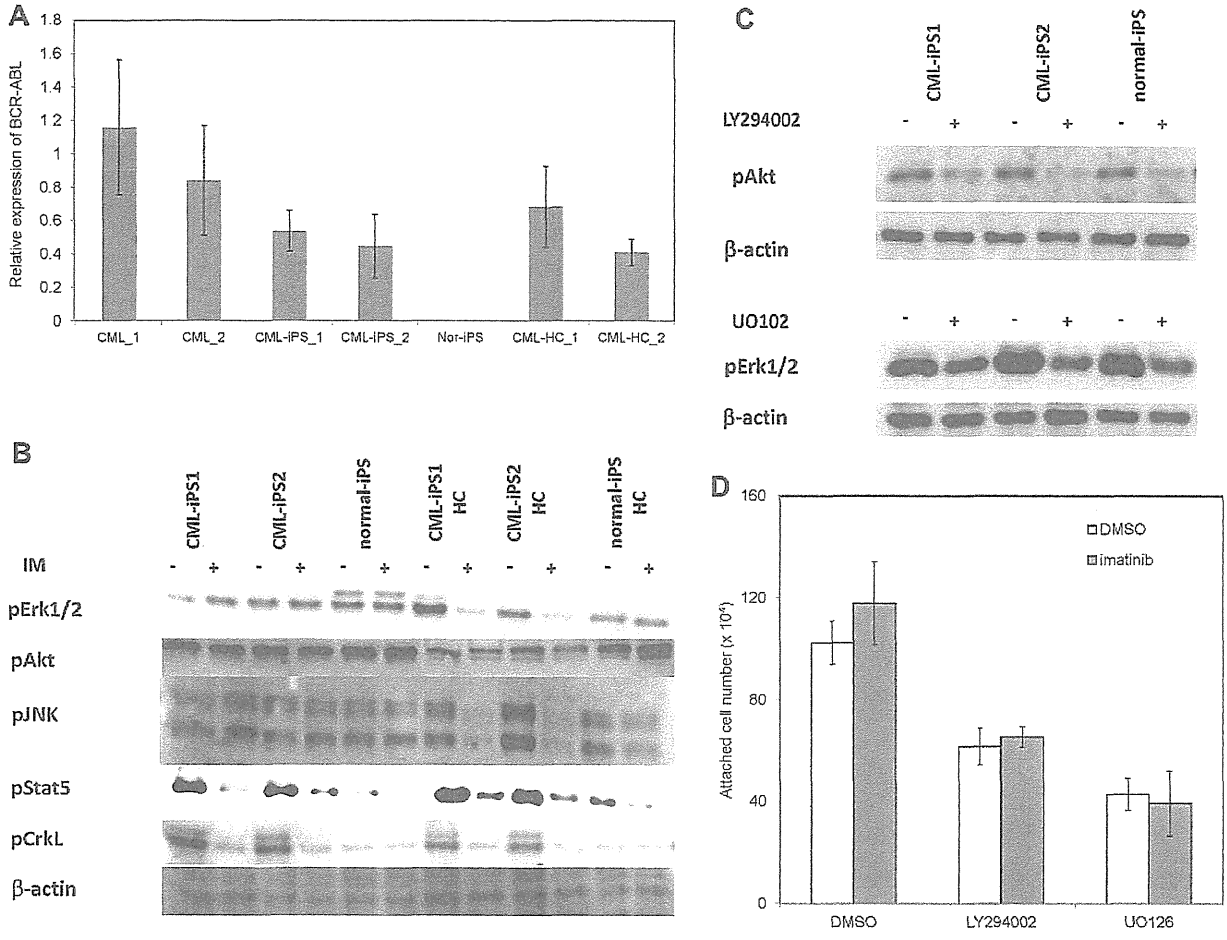

Figure 6. The mechanism of imatinib resistance in the CML-iPSCs. (A) The expression profile of BCR-ABL transcript during hematopoietic differentiation. The expression levels of BCR-ABL in the CML-iPSCs were compared with those of primary CML samples (CML_1 and CML_2), CML-iPSC–derived CD34$^+$ hematopoietic cells (CML-HC_1 and CML-HC_2), and normal iPSC (nor-iPS). The expression level of the mean in the primary CML sample was set at 1. (B) BCR-ABL signaling was estimated in the CML-iPSCs after imatinib (IM) treatment. The phosphorylation state of ERK1/2, AKT, JNK, and STAT5, which are the essential for the survival of BCR-ABL (+) hematopoietic progenitors (CD34$^+$CD45$^+$), were evaluated after imatinib treatment in CML-iPSCs. These were the representative data from 3 independent experiments. (C-D) LY294002 and U0126 (10μM) were added to the culture of CML iPSCs to inhibit AKT and ERK, respectively with or without imatinib. (C) After 4 hours of culture, each inhibitor decreased the phosphorylation of ERK or AKT as expected. (D) The attached cell numbers after treatment with specific AKT or ERK inhibitor were shown. These were the representative data from 3 independent experiments.

The progression of CML from initial indolent CP to the aggressive stages, the AP and BC is caused by additional gene mutations. If we introduce some additional mutation into the CML-iPSCs, the CML BC model may be generated.

Generation of hematologic malignancies derived iPSCs other than CML

Primary samples of hematologic malignancy are usually difficult to be expanded. However, after they are reprogrammed to iPSCs, they can expand unlimitedly. As a result, we can obtain the genetically abnormal hematopoietic cells continuously by redifferentiating them into hematopoietic cells and use them for the studies which require the large number of living cells, such as the analysis for proteome, epigenome, transciptome, leukemia stem cells, or drug screening. Thus, iPSCs technology would be useful for the study of hematologic malignancy based on the patient samples.

However, reprogramming of leukemia cells may be harder than generation of normal iPSCs because of the genetic and epigenetic status of leukemia cells. To overcome the difficulty, application of other factors in addition to the Yamanaka factors may be effective, such as exogenous expression of miRNA-302,[48] chemical compounds, such as azacitidine (DNA metyltranferase inhibitor),[49] BIX01294 (G9a histone metyltransferase inhibitor),[50] VPA (histone deacetylase inhibitor), or TSA (histone deacetylase inhibitor),[26] and knockdown of p53, p21, and Ink4/Arf.[51,52]

In addition, there may be more desirable gene delivery system for iPSC generation for the study of disease pathogenesis. The integration site of retrovirus in the iPSCs may affect the gene expression and change the disease phenotype after redifferentiating them into the original lineages. Recently, efficient induction of transgene free iPSCs, such as using Sendai virus system, was reported[53] and will be applicable for the disease derived iPSCs. We could establish the CML-iPSCs by this system. Using the newly established CML-iPSCs with sendai virus and feeder free culture system, we confirmed the same resistance to imatinib (supplemental Figure 4). Furthermore, without feeder cells, the phosphorylation of ERK and AKT were maintained, although the phosphorylation of STAT5 and CRKL were decreased by imatinib treatment.

In addition, the sendai virus system can be applied to the establishment of other disease derived iPSCs.

Acknowledgments

The authors thank T. Kitamura for pMXs retroviral vector; and Y. Hokama, M. Kobayashi, and Y. Oikawa for expert technical assistance.

This work was supported in part by a Grant-in-Aid for Scientific Research from the Japan Society for the Promotion of Science and by Health and Labor Sciences Research grants from the Ministry of Health, Labor and Welfare, Japan and a grant-in-aid from Core Research for Evolutional Science and Technology of Japan.

Authorship

Contribution: K.K. designed the research, performed experiments, and wrote the paper; S.A., M.H., K.T., N.T., M.O., G.N., K.U., K.N., and Y.K. performed experiments, K.E., H.A., and H.N. discussed the paper; and M.K. conceived and designed the research, supervised the whole project, and wrote the paper.

Conflict-of-interest disclosure: The authors declare no competing financial interests.

Correspondence: Mineo Kurokawa, Deptartment of Hematology and Oncology, Graduate School of Medicine, University of Tokyo, 7-3-1 Hongo, Bunkyo-ku, Tokyo 113-8655, Japan; e-mail: kurokawa-tky@umin.ac.jp.

References

1. Giles FJ, Keating A, Goldstone AH, Avivi I, Willman CL, Kantarjian HM. Acute myeloid leukemia. *Hematology.* 2002;2002(1):73-110.
2. Haferlach T. Molecular genetic pathways as therapeutic targets in acute myeloid leukemia. *Hematology.* 2008;2008(1):400-411.
3. Barabé F, Kennedy JA, Hope KJ, Dick JE. Modeling the initiation and progression of human acute leukemia in mice. *Science.* 2007;316(5824):600-604.
4. Takahashi K, Yamanaka S. Induction of pluripotent stem cells from mouse embryonic and adult fibroblast cultures by defined factors. *Cell.* 2006; 126(4):663-676.
5. Wernig M, Meissner A, Foreman R, et al. In vitro reprogramming of fibroblasts into a pluripotent ES-cell-like state. *Nature.* 2007;448(7151):318-324.
6. Okita K, Ichisaka T, Yamanaka S. Generation of germline-competent induced pluripotent stem cells. *Nature.* 2007;448(7151):313-317.
7. Meissner A, Wernig M, Jaenisch R. Direct reprogramming of genetically unmodified fibroblasts into pluripotent stem cells. *Nat Biotechnol.* 2007; 25(10):1177-1181.
8. Yu J, Vodyanik MA, Smuga-Otto K, et al. Induced pluripotent stem cell lines derived from human somatic cells. *Science.* 2007;318(5858):1917-1920.
9. Takahashi K, Tanabe K, Ohnuki M, et al. Induction of pluripotent stem cells from adult human fibroblasts by defined factors. *Cell.* 2007;131(5): 861-872.
10. Park I-H, Zhao R, West JA, et al. Reprogramming of human somatic cells to pluripotency with defined factors. *Nature.* 2008;451(7175):141-146.
11. Nishikawa S, Goldstein RA, Nierras CR. The promise of human induced pluripotent stem cells for research and therapy. *Nat Rev Mol Cell Biol.* 2008;9(9):725-729.
12. Park I-H, Arora N, Huo H, et al. Disease-specific induced pluripotent stem cells. *Cell.* 2008;134(5): 877-886.
13. Hanna J, Wernig M, Markoulaki S, et al. Treatment of sickle cell anemia mouse model with iPS cells generated from autologous skin. *Science.* 2007;318(5858):1920-1923.
14. Yamanaka S. Strategies and new developments in the generation of patient-specific pluripotent stem cells. *Cell Stem Cell.* 2007;1(1):39-49.
15. Ye L, Chang JC, Lin C, Sun X, Yu J, Kan YW. Induced pluripotent stem cells offer new approach to therapy in thalassemia and sickle cell anemia and option in prenatal diagnosis in genetic diseases. *Proc Natl Acad Sci U S A.* 2009;106(24): 9826-9830.
16. Raya A, Rodriguez-Piza I, Guenechea G, et al. Disease-corrected haematopoietic progenitors from Fanconi anaemia induced pluripotent stem cells. *Nature.* 2009;460(7251):53-59.
17. Carette JE, Pruszak J, Varadarajan M, et al. Generation of iPSCs from cultured human malignant cells. *Blood.* 2010;115(20):4039-4042.
18. Miyoshi N, Ishii H, Nagai K-i, et al. Defined factors induce reprogramming of gastrointestinal cancer cells. *Proc Natl Acad Sci U S A.* 2010;107(1):40-45.
19. Utikal J, Maherali N, Kulalert W, Hochedlinger K. Sox2 is dispensable for the reprogramming of melanocytes and melanoma cells into induced pluripotent stem cells. *J Cell Sci.* 2009;122(19): 3502-3510.
20. Ye Z, Zhan H, Mali P, et al. Human-induced pluripotent stem cells from blood cells of healthy donors and patients with acquired blood disorders. *Blood.* 2009;114(27):5473-5480.
21. Sawyers CL. Chronic myeloid leukemia. *New Engl J Med.* 1999;340(17):1330-1340.
22. Takayama N, Nishimura S, Nakamura S, et al. Transient activation of c-MYC expression is critical for efficient platelet generation from human induced pluripotent stem cells. *J Exp Med.* 2010; 207(13):2817-2830.
23. Hayashi Y, Chan T, Warashina M, et al. Reduction of N-glycolylneuraminic acid in human induced pluripotent stem cells generated or cultured under feeder and serum-free defined conditions. *PLoS One.* 2010;5(11):e14099.
24. Takayama N, Nishikii H, Usui J, et al. Generation of functional platelets from human embryonic stem cells in vitro via ES-sacs, VEGF-promoted structures that concentrate hematopoietic progenitors. *Blood.* 2008;111(11):5298-5306.
25. Okabe M, Otsu M, Ahn DH, et al. Definitive proof for direct reprogramming of hematopoietic cells to pluripotency. *Blood.* 2009;114(9):1764-1767.
26. Huangfu D, Osafune K, Maehr R, et al. Induction of pluripotent stem cells from primary human fibroblasts with only Oct4 and Sox2. *Nat Biotechnol.* 2008;26(11):1269-1275.
27. Chan EM, Ratanasirintrawoot S, Park I-H, et al. Live cell imaging distinguishes bona fide human iPS cells from partially reprogrammed cells. *Nat Biotechnol.* 2009;27(11):1033-1037.
28. Nagae G, Isagawa T, Shiraki N, et al. Tissue-specific demethylation in CpG-poor promoters during cellular differentiation. *Hum Mol Genet.* 2011;20(14):2710-2721.
29. Goyama S, Yamamoto G, Shimabe M, et al. Evi-1 is a critical regulator for hematopoietic stem cells and transformed leukemic cells. *Cell Stem Cell.* 2008;3(2):207-220.
30. Gutiérrez MI, Timson G, Siraj AK, et al. Single monochrome real-time RT-PCR assay for identification, quantification, and breakpoint cluster region determination of t(9;22) transcripts. *J Mol Diagn.* 2005;7(1):40-47.
31. Nishino K, Toyoda M, Yamazaki-Inoue M, et al. DNA methylation dynamics in human induced pluripotent stem cells over time. *PLoS Genet.* 2011;7(5):e1002085.
32. Ishikawa F, Yoshida S, Saito Y, et al. Chemotherapy-resistant human AML stem cells home to and engraft within the bone-marrow endosteal region. *Nat Biotechnol.* 2007;25(11): 1315-1321.
33. O'Brien SG, Guilhot F, Larson RA, et al. Imatinib compared with interferon and low-dose cytarabine for newly diagnosed chronic-phase chronic myeloid leukemia. *New Engl J Med.* 2003; 348(11):994-1004.
34. Druker BJ. Circumventing resistance to kinase-inhibitor therapy. *New Engl J Med.* 2006;354(24): 2594-2596.
35. Jiang X, Zhao Y, Smith C, et al. Chronic myeloid leukemia stem cells possess multiple unique features of resistance to BCR-ABL targeted therapies. *Leukemia.* 2007;21(5):926-935.
36. Steelman LS, Pohnert SC, Shelton JG, Franklin RA, Bertrand FE, McCubrey JA. JAK//STAT, Raf//MEK//ERK, PI3K//Akt and BCR-ABL in cell cycle progression and leukemogenesis. *Leukemia.* 2004;18(2):189-218.
37. Raitano AB, Halpern JR, Hambuch TM, Sawyers CL. The Bcr-Abl leukemia oncogene activates Jun kinase and requires Jun for transformation. *Proc Natl Acad Sci U S A.* 1995; 92(25):11746-11750.
38. Nichols GL, Raines MA, Vera JC, Lacomis L, Tempst P, Golde DW. Identification of CRKL as the constitutively phosphorylated 39-kD tyrosine phosphoprotein in chronic myelogenous leukemia cells. *Blood.* 1994;84(9):2912-2918.
39. Wang X, Lin G, Martins-Taylor K, Zeng H, Xu R-H. Inhibition of caspase-mediated anoikis is critical for basic fibroblast growth factor-sustained culture of human pluripotent stem cells. *J Biol Chem.* 2009;284(49):34054-34064.
40. Brill LM, Xiong W, Lee K-B, et al. Phosphoproteomic analysis of human embryonic stem cells. *Cell Stem Cell.* 2009;5(2):204-213.
41. Mahon F, Delphine R, Guilhot JL, et al. Discontinuation of imatinib in patients with chronic myeloid leukaemia who have maintained complete molecular remission for at least 2 years: the prospective, multicentre stop imatinib (STIM) trial. *Lancet Oncol.* 2010;11(11):1029-1035.
42. Corbin AS, Agarwal A, Loriaux M, Cortes J, Deininger MW, Druker BJ. Human chronic myeloid leukemia stem cells are insensitive to imatinib despite inhibition of BCR-ABL activity. *J Clin Invest.* 2011;121(1):396-409.
43. Hamilton A, Helgason GV, Schemionek M, et al.

Chronic myeloid leukemia stem cells are not dependent on Bcr-Abl kinase activity for their survival. *Blood.* 2012;119(6):1501-1510.

44. Sloma I, Jiang X, Eaves AC, Eaves CJ. Insights into the stem cells of chronic myeloid leukemia. *Leukemia.* 2010;24(11):1823-1833.
45. Zhao C, Blum J, Chen A, et al. Loss of beta-catenin impairs the renewal of normal and CML stem cells in vivo. *Cancer Cell.* 2007;12(6):528-541.
46. Ding VMY, Ling L, Natarajan S, Yap MGS, Cool SM, Choo ABH. FGF-2 modulates Wnt signaling in undifferentiated hESC and iPS cells through activated PI3-K/GSK3beta signaling. *J Cell Physiol.* 2010;225(2):417-428.
47. Hu K, Yu J, Suknuntha K, et al. Efficient generation of transgene-free induced pluripotent stem cells from normal and neoplastic bone marrow and cord blood mononuclear cells. *Blood.* 2011; 117(14):e109-e119.
48. Lin S-L, Chang DC, Lin C-H, Ying S-Y, Leu D, Wu DTS. Regulation of somatic cell reprogramming through inducible mir-302 expression. *Nucleic Acids Res.* 2011;39(3):1054-1065.
49. Han J, Sachdev PS, Sidhu KS. A combined epigenetic and non-genetic approach for reprogramming human somatic cells. *PLoS One.* 2010;5(8): e12297.
50. Plews JR, Li J, Jones M, et al. Activation of pluripotency genes in human fibroblast cells by a novel mRNA based approach. *PLoS One.* 2010; 5(12):e14397.
51. Li H, Collado M, Villasante A, et al. The Ink4/Arf locus is a barrier for iPS cell reprogramming. *Nature.* 2009;460(7259):1136-1139.
52. Utikal J, Polo JM, Stadtfeld M, et al. Immortalization eliminates a roadblock during cellular reprogramming into iPS cells. *Nature.* 2009;460(7259): 1145-1148.
53. Seki T, Yuasa S, Oda M, et al. Generation of induced pluripotent stem cells from human terminally differentiated circulating T cells. *Cell Stem Cell.* 2010;7(1):11-14.

blood

2012 119: 6382-6393
Prepublished online May 9, 2012;
doi:10.1182/blood-2011-12-399659

Inhibition of PAI-1 induces neutrophil-driven neoangiogenesis and promotes tissue regeneration via production of angiocrine factors in mice

Yoshihiko Tashiro, Chiemi Nishida, Kaori Sato-Kusubata, Makiko Ohki-Koizumi, Makoto Ishihara, Aki Sato, Ismael Gritli, Hiromitsu Komiyama, Yayoi Sato, Takashi Dan, Toshio Miyata, Ko Okumura, Yuichi Tomiki, Kazuhiro Sakamoto, Hiromitsu Nakauchi, Beate Heissig and Koichi Hattori

Blood (print ISSN 0006-4971, online ISSN 1528-0020), is published weekly by the American Society of Hematology, 2021 L St, NW, Suite 900, Washington DC 20036.

Inhibition of PAI-1 induces neutrophil-driven neoangiogenesis and promotes tissue regeneration via production of angiocrine factors in mice

Yoshihiko Tashiro,[1,2] Chiemi Nishida,[1] Kaori Sato-Kusubata,[3] Makiko Ohki-Koizumi,[1] Makoto Ishihara,[1] Aki Sato,[1] Ismael Gritli,[1] Hiromitsu Komiyama,[1,2] Yayoi Sato,[1] Takashi Dan,[4] Toshio Miyata,[4] Ko Okumura,[5] Yuichi Tomiki,[2] Kazuhiro Sakamoto,[2] Hiromitsu Nakauchi,[1] *Beate Heissig,[1,3,5] and *Koichi Hattori[1,5]

[1]Center for Stem Cell Biology and Regenerative Medicine, Institute of Medical Science at the University of Tokyo, Tokyo, Japan; [2]Department of Coloproctological Surgery, Juntendo University Faculty of Medicine, Tokyo, Japan; [3]Department of Stem Cell Dynamics, Center for Stem Cell Biology and Regenerative Medicine, Institute of Medical Science at the University of Tokyo, Tokyo, Japan; [4]United Centers for Advanced Research and Translational Medicine, Tohoku University Graduate School of Medicine, Sendai, Japan; and [5]Atopy (Allergy) Center, Juntendo University School of Medicine, Tokyo, Japan

Plasminogen activator inhibitor-1 (PAI-1), an endogenous inhibitor of a major fibrinolytic factor, tissue-type plasminogen activator, can both promote and inhibit angiogenesis. However, the physiologic role and the precise mechanisms underlying the angiogenic effects of PAI-1 remain unclear. In the present study, we report that pharmacologic inhibition of PAI-1 promoted angiogenesis and prevented tissue necrosis in a mouse model of hind-limb ischemia. Improved tissue regeneration was due to an expansion of circulating and tissue-resident granulocyte-1 marker (Gr-1$^+$) neutrophils and to increased release of the angiogenic factor VEGF-A, the hematopoietic growth factor kit ligand, and G-CSF. Immunohistochemical analysis indicated increased amounts of fibroblast growth factor-2 (FGF-2) in ischemic gastrocnemius muscle tissues of PAI-1 inhibitor-treated animals. Ab neutralization and genetic knockout studies indicated that both the improved tissue regeneration and the increase in circulating and ischemic tissue-resident Gr-1$^+$ neutrophils depended on the activation of tissue-type plasminogen activator and matrix metalloproteinase-9 and on VEGF-A and FGF-2. These results suggest that pharmacologic PAI-1 inhibition activates the proangiogenic FGF-2 and VEGF-A pathways, which orchestrates neutrophil-driven angiogenesis and induces cell-driven revascularization and is therefore a potential therapy for ischemic diseases. (*Blood*. 2012;119(26): 6382-6393)

Introduction

Approximately 500 to 1000 people per million per year are diagnosed with critical ischemia of the limb, which in most cases results in serious morbidity and mortality. Therapeutic restoration of blood flow by, for example, the induction of the formation of new capillaries (angiogenesis) is the ultimate goal for critical limb ischemia patients. Growth of new blood vessels in the adult occurs through angiogenesis or arteriogenesis (vessel maturation via recruitment of smooth muscle cells) and vasculogenesis (mobilization of BM-derived cells).[1,2] In contrast to promising results from animal studies, administration of proangiogenic factors such as fibroblast growth factor 2 (FGF-2, also known as basic FGF) or VEGF-A failed to induce significant improvement in ischemia in several phase 1 clinical trials.[3]

The plasminogen activation system and matrix metalloproteinases (MMPs), which can cleave growth factors, growth factor receptors, and adhesion molecules and mediate the extracellular matrix degradation that is necessary for cell migration, are widely recognized as being involved in the process of angiogenesis.[2,4] Although plasminogen activator inhibitor-1 (PAI-1) is one of the primary regulators of the fibrinolytic system, it also has dramatic effects on cell adhesion, detachment, and migration[5] and can inhibit cellular migration by affecting cell adhesion.[6,7] PAI-1–deficient (PAI-1$^{-/-}$) mice showed improved vascular wound healing in models of perivascular electric or transluminal mechanical injury[8] due to improved migration of PAI-1$^{-/-}$ smooth muscle cells. The 52-kDa serine protease inhibitor PAI-1 is the major plasma inhibitor of urokinase-type plasminogen activator (uPA) and tissue-type plasminogen activator (tPA) and inhibits plasmin-mediated fibrinolysis.[9] Studies in mice have indicated that the PAI-1 mRNA concentration is high in the heart, lung, aorta, and adipose and muscle tissue.[10] Plasma and tissue concentrations of PAI-1 increase under pathologic conditions. This increase is mediated by many factors, including reactive oxygen species. PAI-1 is secreted from endothelial cells after ischemia, such as that which occurs in acute myocardial infarction, atherosclerosis, and restenosis.[11,12] However, the role of PAI-1 in both promoting and inhibiting vascular remodeling or tissue regeneration and tumor growth or neoangiogenesis is controversial.[13-15]

The proteases plasmin and MMP-3 cleave and inactivate PAI-1.[16,17] The balance between PAI-1 inhibition of plasmin and other proteases and the cleavage of PAI-1 by these proteases, my play a critical role in the modulation of vascular proliferative responses. However, the exact mechanisms by which PAI-1 affects ischemic tissue regeneration and cell migration are not completely understood. In the present study, we demonstrate that, under ischemic conditions, drug-induced PAI-1 inhibition accelerates neoangiogenesis in a model of hind-limb (HL) ischemia. Moreover, PAI-1 inhibition also increases the proangiogenic factors FGF-2 and VEGF-A, the hematopoietic growth factor kit ligand (KitL), and G-CSF. tPA and MMP-9 deficiency and VEGF-A and FGF-2

Submitted December 21, 2011; accepted May 6, 2012. Prepublished online as *Blood* First Edition paper, May 9, 2012; DOI 10.1182/blood-2011-12-399659.

*B.H. and K.H. share senior authorship.

The online version of this article contains a data supplement.

The publication costs of this article were defrayed in part by page charge payment. Therefore, and solely to indicate this fact, this article is hereby marked "advertisement" in accordance with 18 USC section 1734.

blockade reversed the PAI-1 inhibitor-mediated improved neovascularization and neutrophil recruitment in the peripheral blood and locally within the ischemic tissue/niche. Remarkably, adoptive transfer of ischemic muscle-derived neutrophils derived from PAI-1 inhibitor-treated mice enhanced revascularization. Pharmacologic PAI-1 blockade under ischemic conditions not only increased the absolute number of granulocyte-1 marker (Gr-1$^+$) myeloid cells, but also enhanced their angiogenic performance.

These data provide a fundamental insight into how PAI-1 conditioning of the ischemic niche induces leukocyte influx and controls angiogenesis and suggest that PAI-1 inhibition using small-molecule inhibitors could be a promising cellular target for the treatment of ischemic diseases.

Methods

Animal studies

MMP-9$^{+/+}$ and MMP-9$^{-/-}$ mice and tPA$^{+/+}$ and tPA$^{-/-}$ mice were each used after > 10 back crosses onto a C57BL/6 background. C57BL/6 mice were purchased from SLC. C57BL/6 mice that express GFP under a β-actin promoter were used for transplantation experiments at the age of 6-8 weeks. Animal studies were approved by the animal review board of Juntendo University.

PAI-1 inhibitor

The recently described PAI-1 inhibitor TM5275, 5-chloro-2-((2-(4-(diphenylmethyl) piperazin-1-yl)-2-oxoethoxy acetyl)amino]benzoate, provided by T.M. inhibited PAI-1 activity with a half-maximal inhibition (IC_{50}) value of 6.95μM, as measured by assay of tPA-dependent hydrolysis of a peptide substrate. The IC_{50} values of TM5007 and PAI-749 are 5.60, and 8.37μM, respectively.[18] In vitro, TM5275 (up to 100μM does not interfere with other serpin/serine protease systems such as alpha$_1$-antitrypsin/trypsin and alpha$_2$-antiplasmin/plasmin). Therefore, its PAI-1–inhibitory activity appears to be specific. Preincubation of PAI-1 with TM5275 abolishes detection of the covalent PAI-1–tPA complex by SDS-PAGE.[18] Oral administration of 50 mg/kg of TM5275 to mice resulted in a maximum plasma concentration after 1 hour. The highest plasma drug concentration observed was 6.9 mol/L and the terminal phase half-life of the drug was 6.5 hours. No effect of TM5275 on platelet aggregation induced by ADP and collagen was observed 2 hours after oral administration (10 mg/kg).

Study design

The PAI-1 inhibitor was resuspended in 200 μL of 0.5% carboxymethylcellulose (MP Biomedicals) and administered orally (10 mg/kg body weight) daily to mice with or without induction of HL ischemia from days 0-6. Control mice received vehicle (200 μL of 0.5% carboxymethylcellulose). Recombinant tPA (Eizai) resuspended in 150 mL of 0.2% BSA (Sigma-Aldrich) was administered (10 mg/kg body weight) to mice by daily IP injections from days 0-2.[19]

HL model

Mice were anesthetized with pentobarbital sodium (40 mg/kg body weight) that was given intraperitoneally. Briefly, an incision was made in the skin on the medial aspect of the left thigh. The femoral artery was ligated using 4-0 silk sutures (Ethicon) and cut immediately distal to the inguinal ligament and proximal to the popliteal bifurcation site. Changes in blood flow were recorded at days 0, 1, 4, 7, 14, and 21 after the procedure using a laser Doppler perfusion image analyzer (Moor Instruments). Blood was collected via retroorbital bleeding using heparin-coated and plain capillary tubes and WBCs were counted. Plasma and serum samples were stored at −30°C. Mice were killed 1, 5, 15, and 21 days after resection of the femoral artery.

Isolation of Gr-1 cells from muscle tissue after HL ischemia induction

Muscle-derived Gr-1$^+$ cells were isolated from HL-ischemia–induced C57BL/6 mice treated with or without PAI-1 inhibitor on day 5 using MACS. In brief, muscles were excised and cut into small pieces. After excision, tissue pieces were lysed with a buffer containing 20mM Tris-HCl, 5mM EDTA, 1% collagenase II, 2.4 U/mL of Dispase, 1mM PMSF, and 10 μmol pepstatin for 1.5 hours. Gr-1$^+$ and Gr-1$^-$ cells were isolated using the anti–Ly-6G Microbead kit (Miltenyi Biotec). Cell morphology was determined on cytospins after Wright-Giemsa staining.

In vivo blocking experiments

HL-ischemic mice treated with or without the PAI-1 inhibitor (days 0-6) were coinjected intraperitoneally with 10 μg of anti–mouse VEGF-A (AF-493-NA; R&D Systems) or 10 μg of goat specific anti–human FGF-2 (AF-233-NA; R&D Systems) on day 0. Appropriate isotype Ab controls were included.

Transplantation of PAI-1 inhibitor-mobilized Gr-1$^+$ cells

Muscle-derived Gr-1$^+$ cells were isolated from HL-ischemia–induced C57BL/6 donor mice treated with or without PAI-1 inhibitor on day 5 by FACS using a FACSCalibur flow cytometer (BD Biosciences). Gr-1$^+$ cells (5×10^4 cells/injection/d) were injected daily intramuscularly into C57BL/6 recipient mice on days 0 and 1 after HL ischemia induction.

Flow cytometry

PBMCs were stained with the following Abs: CD45-FITC (1:200, clone 30-F11; BD Pharmingen), CD11b-APC (1:200, clone M1/70; BD Pharmingen), and Gr-1-PE (1:200, clone RB6-8C5; BD Pharmingen). Cells were analyzed by FACS.

Histological assessment

Ischemic adductor or, if indicated, hamstring (posterior thigh) muscle tissue samples were snap-frozen in liquid nitrogen. Transverse cuts of the whole leg were prepared. Sections were stained with H&E.

Tissue sections were washed, serum blocked, and stained with the first Ab overnight at 4°C. Muscle sections were stained with the anti-CD31 Ab (clone T-2001; BMA Biomedicals) followed by biotin-conjugated goat anti–rat IgG (Vector Laboratories) and FITC-conjugated streptavidin (Alexa Fluor 488; Molecular Probes). In addition, tissues were stained with the primary anti–mouse FGF-2 (clone D0611; Santa Cruz Biotechnology) and FGF-R1 (clone 755639; Abcam) and VEGF-A Abs, followed by a goat anti–rabbit IgG Ab conjugated with Alexa Fluor 488 (Molecular Probes). Muscle sections were also stained with anti–mouse VWF Ab (Dako), followed by Cy3-conjugated streptavidin (Alexa Fluor 594; Molecular Probes) using the M.O.M kit (Vector Laboratories) according to the manufacturer's instructions. Neutrophils were identified using the Gr-1 Ab (clone RB6-8C5; R&D Systems), followed by biotin-conjugated goat anti–rat IgG (Vector Laboratories) and Cy3-conjugated streptavidin (Alexa Fluor 594; Molecular Probes) Abs. Macrophages were identified using the F4/80 Ab (clone A3-1; AbD Serotec), followed by biotin-conjugated goat anti–rat IgG (Vector Laboratories) and Cy3-conjugated streptavidin (Alexa Fluor 594; Molecular Probes) Abs. In addition, tissues were stained with the primary anti–mouse VEGF-A Ab (clone A-20; Santa Cruz Biotechnology), followed by the goat anti–rabbit IgG Ab conjugated with Alexa Fluor 488 (Molecular Probes). Nuclei were counterstained with DAPI (Molecular Probes).

RT-PCR analysis

Total RNA was extracted from the gastrocnemius muscle of HL-ischemic or untreated mice using RNA TRIzol (Invitrogen) according to the manufacturer's directions. Briefly, 25 mg of muscle was immediately immersed in 1 mL of TRIzol reagent. The muscle was homogenized on ice using a homogenizer. The aqueous and organic phases were separated using 200 μL

of chloroform. Total RNA was precipitated using 500 μL of isopropyl alcohol, washed 3 times with 75% ethanol, and redissolved in 24 μL of DEPC-treated H_2O. The concentration and purity of the RNA was determined using a UV spectrophotometer by measuring the absorbance at 260 and 280 nm. cDNA was amplified by PCR using the following specific forward and reverse primer pairs: for *uPA*: (5′-GTCCTCTCTGCAACAGAGTC-3′) and (5′-CTGTGTCTGAGGGTAATGCT-3′); for *tPA*: (5′-GTACTGCTTTGTGGACT-3′) and (5′-TGCTGTTGGTAAGTTGTCTG-3′); for *PAI-1*: (5′-AAAGGACTCTATGGGGAGAA-3′) and (5′-TAGGGAGGAGGGAGTTAGAC-3′); and for the *b-actin* control: (5′-TGACAGGATGCAGAAGGAGA-3′) and (5′-GCTGGAAGGTGGACAGTGAG-3′).

ELISA

Plasma and serum samples from PAI-1 inhibitor-treated and untreated mice with HL-ischemia induction were assayed for murine VEGF-A, MMP-9, KitL, G-CSF, PAI-1, and tPA using ELISA kits (R&D Systems, Cell Sciences, and Molecular Innovations).

Western blotting

Muscle tissue extracts were prepared for Western blotting. Briefly, gastrocnemial muscle tissues were lysed in a buffer containing 20mM Tris-HCl, 5mM EDTA, 1% Triton X-100, 1mM PMSF, and 10μM pepstatin after mashing between 2 glass slides. Whole-muscle lysates were subjected to SDS-PAGE (8%), followed by electroblotting onto a PVDF membrane. Membranes were blocked in 20mM PBS and 0.05% Tween-20 (vol/vol) containing 5% (wt/vol) skim milk powder at room temperature, followed by overnight incubation with the anti–PAI-1 Ab (1:1000; Abcam), and an HRP-conjugated secondary Ab (1:20; Nichirei Biosciences) for 1 hour. Membranes were developed using the ECL Plus system (Amersham Life Sciences).

Reverse fibrin zymography

Reverse fibrin zymography, although similar to fibrin zymography, uses agar gels that contain uPA in addition to fibrinogen and plasminogen to determine unbound/free PAI-1. Protein extracts (50 μg) from normal and ischemic muscle tissues were loaded on an 8% acrylamide gel, and, after SDS-PAGE, the SDS was removed by washing the acrylamide gels with distilled water followed by incubation for 2 hours with a buffer containing 2.5% Triton X-100, 0.05 M/L of Tris-HCl (pH 7.5), and 0.1 M/L of NaCl to renature the enzymes. The gels were then incubated for 12-24 hours at 37°C in buffer containing 0.05 M/L of Tris-HCl (pH 7.5) and 0.01 M/L of $CaCl_2$. After this incubation, the gels were stained for 1 hour with Coomassie blue diluted with 50% methanol and 10% acetic acid and decolorized with buffer containing 25% methanol and 8% acetic acid. No fibrinolysis occurs in the area of the gel where the PAI-1 protein is located, resulting in a visible band. Gels were then photographed.

Fibrin plate assay

Plasma fibrinolytic activity was measured using the modified fibrin plate method. Briefly, blood samples were collected in plain tubes containing 3.2% sodium citrate, mixed at a ratio of 9:1, and centrifuged at 3000*g* for 20 minutes at 4°C. The euglobulin fraction was prepared by acidification of 1:10 diluted plasma to pH 5.9 with 0.25% (vol/vol) glacial acetic acid at 4°C, which was then centrifuged at 500*g* at 4°C for 10 minutes. The supernatant was discarded. The euglobulin precipitate was resuspended in an EDTA-gelatin-barbital buffer (pH 7.8), and 30 mL of each sample were placed in identical depressions in a fibrin-agarose plate. Next, 10 mL of a 1.5 mg/mL bovine fibrinogen solution in Barbitol buffer (50mM sodium barbitol, 90mM NaCl, 1.7mM $CaCl_2$, and 0.7mM $MgCl_2$, pH 7.75) and 10 mL of a 1% agarose solution were brought to 45°C in a water bath, and 10 NIH units of thrombin (250 NIH units/mL) were then added into the agarose solution. The fibrinogen and agarose solutions were mixed in a 140-mm Petri dish and kept at room temperature for 2 hours to form fibrin clots. Enzymes were dissolved and diluted to the appropriate concentration in Barbitol buffer. Each enzyme solution (10 mL) was dropped into a hole preformed on the fibrin plate. The plate was incubated at 37°C for 18 hours. The zone of lysis on the fibrin plate (fibrinolytic activity) was measured using Area Manager (Ruka International).

Statistical analyses

All data are presented as means ± SEM. Student *t* tests were performed. $P < .05$ was considered significant.

Results

Ischemia is associated with increased expression of PAI-1 in ischemic muscle tissue

Because oxygen deprivation, such as that which occurs during tissue ischemia, can tip the natural anticoagulant/procoagulant balance,[20] in the present study, we investigated whether the fibrinolytic factors are present within ischemic gastrocnemius muscle tissues. An increase in *PAI-1*, *uPA*, and *tPA* mRNA expression, as determined using quantitative PCR (Figure 1A-C), and an increase in PAI-1 protein and activity, as determined by Western blotting and reverse fibrin zymography, respectively (Figure 1D-E), were detected in ischemic muscle tissues from HL ischemia-induced mice compared with nonischemic controls. These results demonstrated that ischemia increased ischemic muscle PAI-1 activity and simultaneously augmented local fibrinolytic activity.

We next evaluated the effects of administration of the PAI-I inhibitor TM5275 on fibrinolytic factor release into the circulation. The PAI-1 inhibitor TM5275 (hereafter referred to as the PAI-I inhibitor) is an effective novel oral drug that inhibits PAI-1 by preventing binding of PAI-1 to tPA.[18] Both active and latent forms of PAI-1 can circulate.[20] PAI-1 inhibits tPA and uPA and PAI-1 is usually present in excess over tPA in plasma. In the present study, PAI-1 inhibitor treatment administered daily from days 0-6 blocked the systemic increase in active PAI-1 in plasma (Figure 1F) and augmented plasma tPA (Figure 1G) and plasmin levels during HL-ischemic recovery (Figure 1H). When the PAI inhibitor treatment was suspended, plasma tPA and plasmin levels returned gradually to baseline levels in 14-21 days. These data indicate that PAI inhibition during ischemic recovery creates a fibrinolytic state.

Pharmacologic targeting of PAI-1 promotes ischemic revascularization and tissue regeneration.

We next determined the consequences of PAI-1 inhibition for tissue regeneration after HL ischemia induction by treating ischemia-induced C57BL6/C mice with the PAI-1 inhibitor or vehicle control. Foot digit necrosis was prevented in PAI-1 inhibitor-treated animals (Figure 1I). The ischemic limb of PAI-1 inhibitor-treated mice displayed faster perfusion recovery, as determined by laser Doppler perfusion image analysis, than vehicle-treated controls (Figure 1I-J). Smaller areas of necrosis were detected in histochemically stained ischemic muscle tissue sections of the lower and upper limb (ie, the gastrocnemius and hamstring muscles) from PAI-inhibitor treated than from vehicle-treated mice (Figure 1K-N). These data demonstrate that PAI inhibition accelerates ischemic tissue recovery.

Endogenous tPA and MMP-9 are required for the tissue-regenerative effects observed after PAI inhibition

We reported previously that the fibrinolytic factor tPA promotes angiogenesis and tissue regeneration in HL-ischemic tissue, which

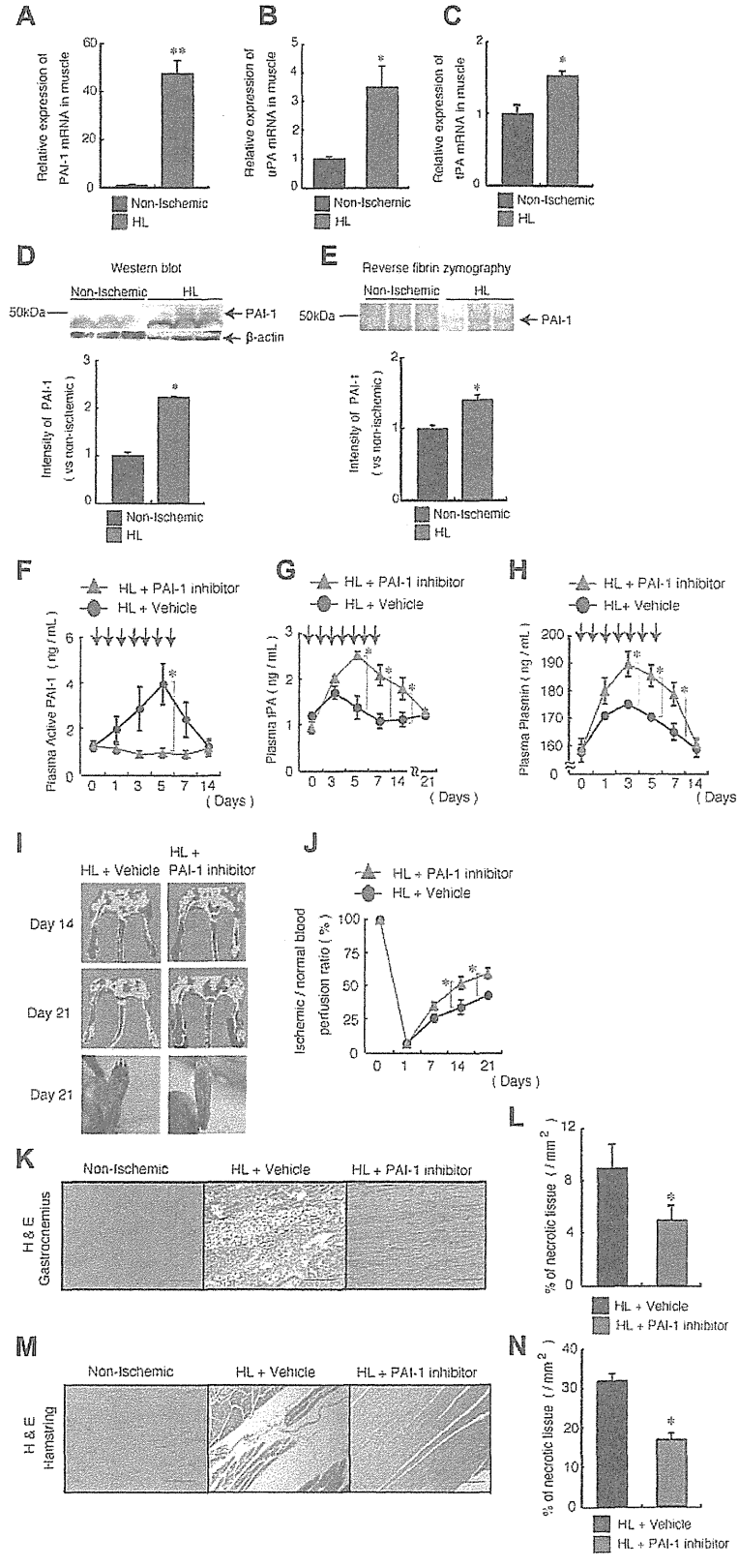

Figure 1. PAI-1 inhibition improves HL-ischemic tissue regeneration. (A-E) C57BL/6 mice were HL treated and gastrocnemius muscles were analyzed on day 1. (A-C) Quantitative RT-PCR analysis of the mRNA expression of *PAI-1* (A), *uPA* (B), and *tPA* (C) in nonischemic and HL-ischemic muscle tissue using β-actin as an internal control (n = 3/group for all experiments). (D-E) Homogenates of ischemic and nonischemic tissues that were harvested on day 1 after HL-ischemia induction in 3 different C57BL/6 mice were assayed for murine PAI-1 protein by Western blot analysis (D) or for PAI activity by reverse fibrin zymography (E). Densitometric analysis is shown (bottom). (F-N) HL ischemia was induced in C57BL/6 mice, followed by oral administration of the PAI-1 inhibitor or vehicle given daily from days 0-6. Arrows indicate when the PAI inhibitor was administered. Plasma levels of active PAI-1 (F), tPA (G), and plasmin (H) were assayed in PAI-1– or vehicle-treated HL-ischemic mice by ELISA (n = 7/group for PAI-1 and tPA; n = 6/group for plasmin). (I-J) Representative macroscopic images (I) and the limb perfusion ratio (ischemic/nonischemic; J) of ischemic limbs after HL-ischemia induction. Macroscopic evaluation of the limbs on day 21 (I, bottom) shows foot-digit necrosis only in HL + vehicle-treated animals (n = 5/group). (K-N) Muscle sections of a nonischemic limb and of gastrocnemius (K-L) and hamstring muscles (M-N) of the ischemic limbs from treated mice were stained with H&E (after 21 days; scale bars, 200 mm; K,M) and necrotic areas were evaluated (n = 4 for vehicle group; n = 3 for PAI-1 inhibitor group; L,N). Data represent means ± SEM. $^*P < .05$; $^{**}P < .001$.

requires the up-regulation of MMP-9.[19] In the present study, we found that PAI-1 inhibitor treatment during ischemic recovery augmented fibrinolytic activity in blood samples from $tPA^{+/+}$ mice, but not from $tPA^{-/-}$ mice (Figure 2A), and augmented MMP-9 plasma levels during HL-ischemic recovery in $tPA^{+/+}$ mice compared with vehicle-treated $tPA^{+/+}$ mice, suggesting that increased tPA and MMP-9 may mediate the observed effects of PAI-I (Figure 2B). No change in MMP-9 plasma levels was observed in